

Review

An Overview of Light-Assisted CO₂ Cycloaddition for Cyclic Carbonate: Paths of Photo-Induced Thermal-Catalysis, Photocatalysis and Photo-Thermal Synergistic Catalysis

Bin Zhu¹, Qichao Cao¹, Xin Ding^{1,*}, and Xiaolong Yang^{1,2,*}¹ School of Chemistry and Chemical Engineering, Qingdao University, 308 NingXia Road, Qingdao 266071, China² State Key Laboratory of Bio-Fibers and Eco-Textiles, Collaborative Innovation Center of Shandong Marine Bio-Based Fibers and Ecological Textiles, Qingdao University, 308 NingXia Road, Qingdao 266071, China

* Correspondence: dingxin@qdu.edu.cn (X.D.); yangxl@qdu.edu.cn (X.Y.)

Received: 4 November 2024; Revised: 6 January 2024; Accepted: 22 January 2025; Published: 6 February 2026

Abstract: The increase of CO₂ concentration significantly results in severe greenhouse effect. Reducing emission and chemically utilizing CO₂ are effective means to solve this problem. CO₂ cycloaddition reaction with epoxide is atomically economical and environmentally friendly. However, current catalytic systems still have a long way to go for high catalytic efficiency under mild conditions. Solar energy has demonstrated excellent characteristics in direct photothermal utilization, photocatalytic reactions, and photoelectrochemical reactions recently. Therefore, herein this review summarizes the research work on solar energy mediated CO₂ cycloaddition reactions in the past decade. Firstly, the heat generated by photothermal effects is confined to the local space and can be more effectively absorbed by reaction molecules for efficient reactions, greatly reducing the energy consumption of traditional thermal reactions. CO₂ cycloaddition with carbon-based materials, polyoxometalates (POM), metal organic frameworks (MOFs), covalent organic frameworks (COFs), and ionic liquids (ILs) as catalysts are reviewed and analyzed; Secondly, semiconductor exhibit high activity due to activation of reactants by photogenerated charges and holes. Single atom catalysts, composites, atomic clusters, MOFs, COFs, Porous organic polymers (POPs), and others used in such reaction are reviewed and analyzed; Finally, the solar light mediated photothermal synergistic catalysis and the reaction system of light and external heating synergy are introduced and analyzed. Last but not least, some issues in the development of solar energy mediated CO₂ cycloaddition reactions are analyzed and discussed, and future research prospects are proposed on this basis.

Keywords: heterogenous CO₂ cycloaddition; photo-induced thermal-catalysis; photocatalytic CO₂ cycloaddition; photothermal synergistic catalysis; cyclic carbonate

1. Introduction

In the history of human being's development, the Industrial Revolution lasted for over 200 years is like a double-edged sword. On the one hand, it has brought advanced productivity to humanity, creating today's prosperity and advanced way of life. However, on the other hand, the rapid consumption and imprecise processing of nonrenewable fossil resources have cast a shadow over the sustainable development of energy and environment in the future. The greenhouse effect induced by greenhouse gas like CH₄ and CO₂ etc. severely threatens human beings. The average concentration of CO₂ in the atmosphere achieved 419.47 ppm in January 2023, which was almost 1.55 times that of pre-industrial times (~270 ppm). Over the past thirty years, global CO₂ emissions have doubled and are expected to double by 2040 (Figure 1) [1]. The United States and China account for 20.3% and 20.0% respectively, accounting for 40.3% of the global total.

Given this severe situation, countries around the world attach great importance to the excessive emissions of CO₂ and the resulting extreme climate problems. Specifically, countries have successively signed and implemented the United Nations Framework Convention on Climate Change (1992), the Kyoto Protocol (1997), the Bali Roadmap (2007), and the Paris Agreement (2015). The Paris Agreement aims to limit the increase in global average temperature to well below 2 °C relative to pre-industrial levels, with an aspiration to restrict the rise to



under 1.5 °C compared to those same levels (Figure 1B) [2]; By 2030, global carbon emissions will be controlled at 40 billion tons, achieving net zero emissions by 2080; all parties will make effort to such action to address climate change through “independent contributions”. The Paris Agreement is an important milestone in global climate management, marking the beginning of global cooperation to address the climate issues facing humanity.

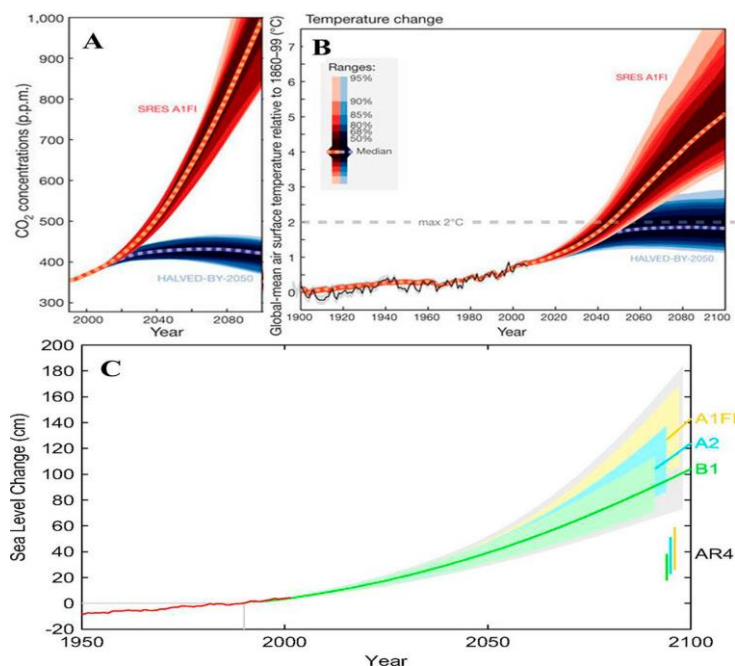


Figure 1. (A) Levels of CO₂ in the atmosphere and (B) global average temperature of surface air for the Special Report on Emissions Scenarios (SRES) fossil intensive (A1FI) and HALVED-BY-2050 (halving the 1990 global Kyoto-gas emissions by 2050) scenarios. Reprinted with permission from Ref. [1]. Copyright 2009 Springer Nature. (C) Changes in sea level projected from 1990 to 2100. Reprinted with permission from Ref. [2]. Reprinted with permission from Ref. [3], Copyright 2019 American Chemical Society.

As a result, the concept of global carbon neutrality emerges as the times require. Several strategies have been proposed and implemented to achieve carbon neutrality. For instances, carbon capture and storage (CCS or CCUS) technique, that is capturing, storing, or utilizing of CO₂ [4,5]. For storage, it means capturing and releasing CO₂ into the atmosphere, compressing it, and then returning it to depleted oil fields, natural gas fields, or other safe underground locations. However, at least there are two problems hinders the ideal carbon storage, firstly the cost of carbon capture and storage is very high, including the transportation, compression, and search and evaluation of safe locations for CO₂. Another reason is that no one knows if this technology is really that effective. Or, in other words, whether deeply buried CO₂ will leak under extreme geological movements is a problem. Comparatively speaking, a more promising approach than carbon storage is to purposefully utilize CO₂ as a renewable raw material to generate high value-added products and fuels, and even convert CO₂ into chemicals and fuels using renewable resources [6,7]. This not only allows intermittent renewable energy to be stored in chemicals for convenient transportation and efficient utilization, but also realizing a circular carbon economy.

In classic review paper of T. Sakakura, they proposed four methods for CO₂ transformation [8]. In other words, high-energy reactants react with CO₂ under the action of an external energy field to produce low-energy products, while promoting the reaction equilibrium to shift towards the product side can accelerate the reaction rate. High-energy reactant, low-energy product, energy and reaction equilibrium contribute to the transformation of CO₂. The roadmap of CO₂ transformations is presented in Figure 2, among them five transformation paths have been industrialized, specifically, these are synthesizing urea (1921), methanol, cyclic carbonate (1958), linear carbonate polymer and salicylic acid (1890). Nevertheless, industrial utilization accounts for only 0.5% of the total anthropogenic CO₂ emissions [9]. All these process routes are driven by heterogeneous thermal catalysis. We searched the Web of Science with keywords of CO₂ conversion or CO₂ catal* or CO₂ reduction in the past decades (2014–2024) as shown in Figure 3A. It is found that the number of research papers has skyrocketed since 2019. As of 2023, 137,302 papers on CO₂ catalytic conversion have been published worldwide. In depth, research papers contributed by China accounts for 31.58% of the total, much higher than the second ranked United States (17.83%), followed by Germany, The United Kingdom, Japan, and India in terms of the overall number of published articles shown in Figure 3B.

The transformation path of CO₂ can be categorized to thermal catalysis, photocatalysis, electrocatalysis and biological transformation [10]. Specifically, types of chemical reaction of conversion are divided into carboxylation, hydrogenation, reduction, cycloaddition, reforming and biological synthesis. CO₂ cycloaddition reaction attracts extensive attention because of its inherent merits: (1) as above mentioned [11,12], it is proposed by T. Sakakura and widely accepted that high-energy reactants like epoxide is beneficial for CO₂ transformation; (2) low-energy synthetic targets such as organic carbonate is either beneficial for CO₂ transformation; (3) bond energy of C=O is as high as 799 kJ/mol, conventional activation methods face the problem of difficulty in breaking carbon oxygen bonds and activating CO₂, Fortunately, based on the above (1) and (2) advantages, the energy released by ring opening of epoxide perfectly compensate energy required for CO₂ activation, so the reaction does not require extremely high energy intervention; (4) CO₂ cycloaddition is 100% atomic economy and no atom is wasted, which guarantees the loop-closed management of carbon cycle; (5) Cyclic carbonates are stable liquids that are beneficial for long-term storage of CO₂ [13]; (6) the synthesizing target cyclic organic carbonates (ethylene carbonate (EC), propylene carbonate (PC)) are superior solvents in chemical industrial and batteries field, useful intermediates for synthesizing acyclic carbonates, carbamates, polymers, methanol, cis-diols, spiro compounds, heterocyclic compounds, and ILs [14].

Therefore, such reaction attracts extensive research interests from both academia and industry. For example, Shell Omega process utilizes the hydrolysis of ethylene carbonate obtained from cycloaddition reaction to produce ethylene glycol [15]. Asahi Kasei uses ethylene carbonate and methanol cracking to produce dimethyl carbonate (polycarbonate precursor) and ethylene glycol simultaneously [16]. The global market of cyclic carbonate in 2020 is 3.5 billion and it is forecasted to achieve 7.1 billion in 2030, growing at a Compounded Average Growth Rate (CAGR) of 7.2% [17]. We searched the Web of Science with keywords of CO₂ cycloaddition or CO₂ cyclic carbonate in the past decades (2014–2024) as shown in Figure 3C. It is found that the number of research papers has surged since 2012 and continues to grow exponentially every year. There are 3533 papers published at 2024. As of 2024, 6255 papers on CO₂ cycloaddition have been published worldwide. In addition, research papers contributed by China accounts for 48.4% of the total, much higher than that of others Figure 3D.

CO₂ and epoxides can generate small-molecule cyclic carbonates or high-molecular-weight polymer molecules Under different catalysts and reaction conditions, which may lead to the generation of reaction selectivity. The essence of this product selectivity depends on the epoxide molecule itself, the catalyst, the cocatalyst or the reaction conditions. From the perspective of the structure of the epoxide molecule itself, aliphatic epoxides such as PO (Propylene oxide) are more likely to generate cyclic carbonates. Darensbourg analyzed from a thermodynamic perspective and believed that PC (Propylene carbonate) has good thermal stability and a small difference in activation energy compared to PPC (Poly propylene carbonate); while alicyclic epoxides have rigid six-membered rings, and the cyclic by-product cyclohexene carbonate CHC has a large ring strain and poor thermal stability, with a large difference in activation energy compared to the formation of polycarbonate cyclohexene PCHC (Figure 4A,B) [18].

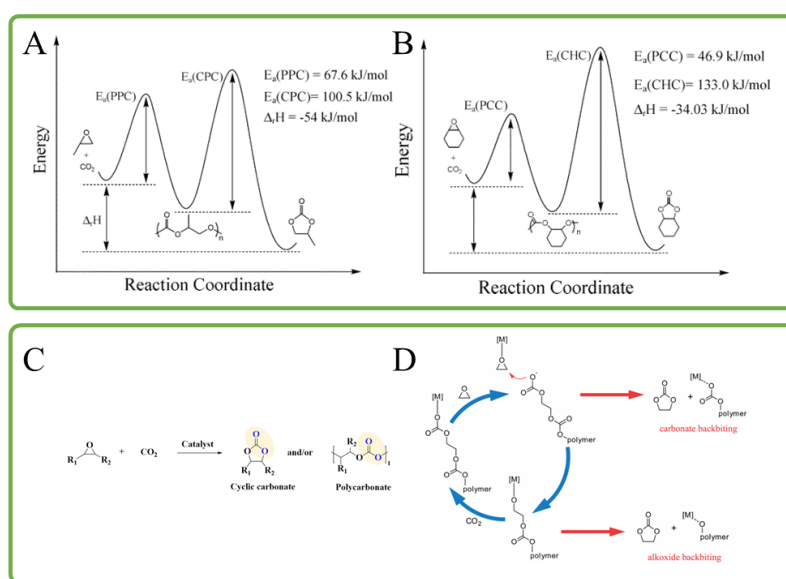


Figure 4. (A,B) are the reaction coordinate diagrams for the coupling of CO₂ with PO and CHO. Reprinted with permission from Ref. [18]; (C) CO₂ cycloaddition reaction equation; (D) Reaction mechanism of cyclic carbonate side reaction. Reprinted with permission from Ref. [19].

Therefore, under the same catalytic conditions, for the target product of cyclic carbonates, the product selectivity of PO is generally higher than that of CHO. There is also the issue of product selectivity in the CO₂/epoxide copolymerization process, but at this time, the cyclic carbonate is generally a by-product. During the chain growth process, the active alkoxide anion and the carbonate anion undergo a “back-biting” mechanism to close the ring and form a five-membered cyclic carbonate (Figure 4C,D). This process is more likely to occur when the viscosity of the system increases and mass transfer is hindered in the later stage of the polymerization [19]. In addition, low temperature is conducive to polymerization, while high temperature is favorable for depolymerization to form cyclic carbonates. The formation of copolymers and cyclic carbonates is respectively controlled by kinetics and thermodynamics. Moreover, increasing the proportion of cocatalysts such as quaternary ammonium salts and reducing the pressure of CO₂ will both lead to an increase in the proportion of cyclic carbonates.

In this context, review papers on the CO₂ cycloaddition reaction have sprung up, particularly focusing on thermal-catalytic materials such as MOFs [20–22], COFs [23–25], POMs [26,27], ILs (Ionic liquids) [28,29] and metal–organic complexes [30], respectively (Figure 5). Simultaneously, the last rule of CO₂ transformation methodologies state that providing physical energy -light or electricity- is further beneficial for the transformation reaction. Therefore, light as external energy source can promote the conventional thermal-catalysis of CO₂ cycloaddition. However, few reviews have summarized in focusing on light-assisted CO₂ cycloaddition reaction have been published so far, especially categorizing catalytic systems by the routes of photo-induced thermal catalysis, photocatalysis, and photo-thermal synergistic catalysis (Figure 6). Therefore, in consideration of indispensable role of clean solar energy in CO₂ chemical utilization, it is highly necessary to present timely comprehensive and cutting-edge review paper on “An Overview of Light-assisted CO₂ Cycloaddition for Cyclic Carbonate: Paths of Photo-induced Thermal-catalysis, Photocatalysis and Photo-thermal synergistic catalysis”.

Herein, we present a leading-edge timely and comprehensive review on development of light-assisted CO₂ cycloaddition during the last decade, mainly focusing on photo-induced thermal-catalysis system, pure photo-catalysis system and bifunctional photo-thermal synergistic catalysis system. Firstly, the background of CO₂ emission and strategy of chemical utilization of CO₂ is elucidated (Section 1). Subsequently, photo-induced thermal-catalysis system is discussed, and some influential works are presented and discussed, including carbon-based material, single atom catalyst, POMs, MOFs, COFs and omnipotent ILs etc. (Section 2); In addition, CO₂ cycloaddition realized by sole photocatalysis has also been discussed, mainly including SACs (Single atom catalysts), atomic cluster, composites and organic framework material (Section 3); Next, some catalytic system employed both photothermal effect and photoinduced carriers (holes and electron) is summarized and discussed either (Section 4); Finally, we analyze the current research directions and existing problem (Table 1), outlook the future research and identify the research questions that should be focus on in the future (Section 5). The above-mentioned information paves the way for exploring new highly efficient CO₂ cycloaddition catalytic system driven by clean solar energy.

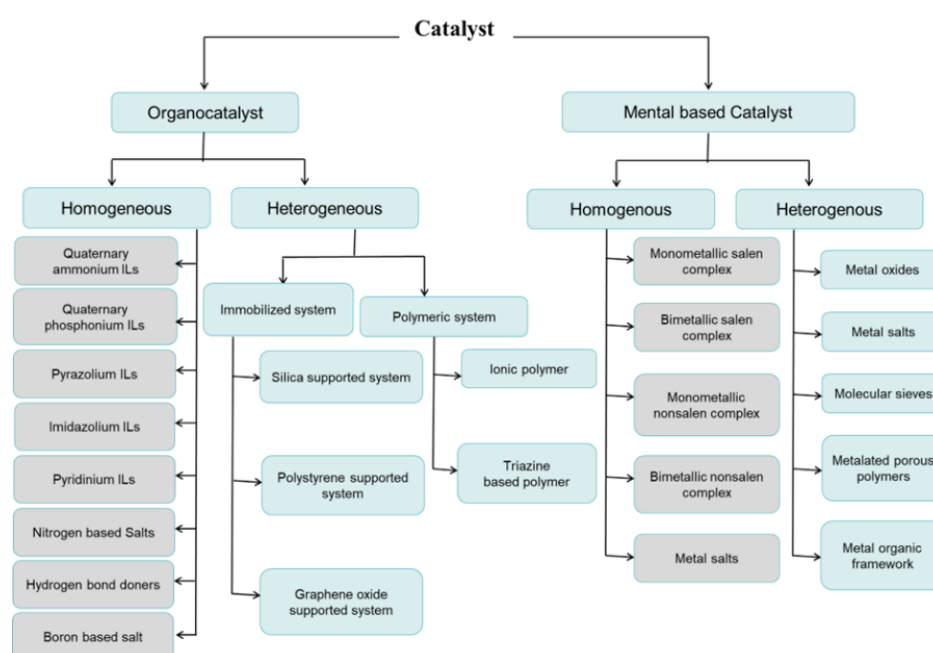


Figure 5. Classification of catalysts for cyclic carbonates [17], Copyright 2024 Elsevier.

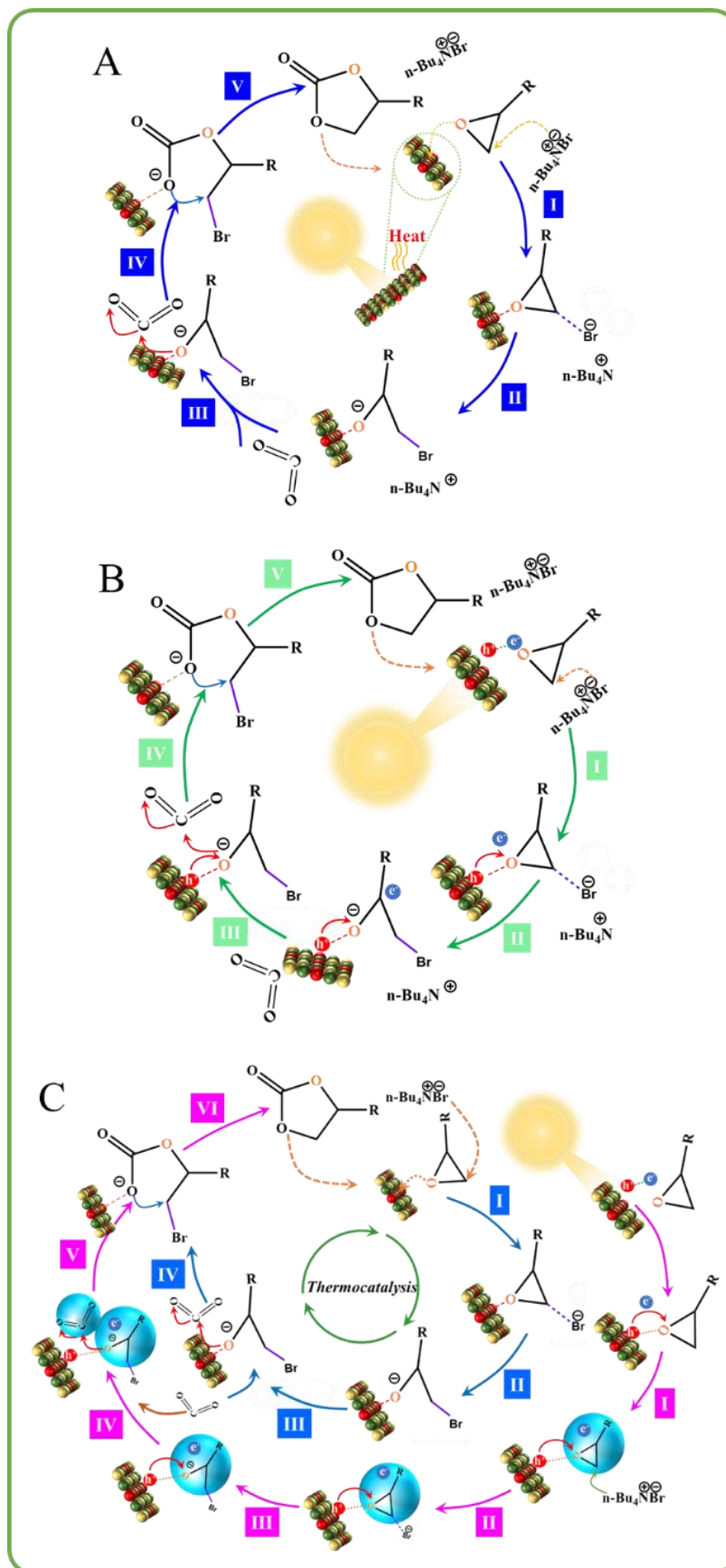


Figure 6. (A) Photo-induced Thermal-catalysis reaction mechanism; (B) Photocatalytic reaction mechanism; (C) Photo-thermal synergistic catalysis reaction mechanism.

Table 1. The advantages, disadvantages, and challenges of photocatalysis, photo-induced Thermal-catalysis, and Photo-thermal synergistic catalysis.

Style	Source of Heat	Essential	Advantages	Disadvantages	Challenges
Photocatalysis	None	Photocatalysis	Energy-saving	(1) Limited to semiconductor; (2) Low efficiency	Catalytic activity is limited by carriers' separation kinetics.
Photo-induced thermal catalysis	Photon	Thermalcatalysis	Energy-saving	(1) Sufficiently high light intensity is required (usually >1000 mW/cm ²); (2) Photothermal material with high photo-to-thermal conversion efficiency is needed.	Realize the unification of catalytic active sites and photothermal material.
Photo-thermal synergistic catalysis	Photon	Photocatalysis+ thermalcatalysis	Energy-saving high efficiency	Modulate the balance of photocatalyst and photothermal material	(1) Catalytic activity is limited by carriers' separation kinetics. (2) Realize the unification of catalytic active sites and photothermal material.
	External heating	Photocatalysis+ thermalcatalysis	Energy-saving high efficiency	Catalytic activity is limited by carriers' separation kinetics.	Unify the photocatalytic unit and the thermal catalytic unit.

2. Photo-Induced Thermal-Catalysis

Solar thermochemistry has the potential to utilize the entire solar spectrum, which covers a wide range of wavelengths from over 300 to over 1000 nm. Both visible and infrared light can interact with materials to produce photothermal effects. Therefore, the oldest and most direct way to utilize solar energy is to utilize its thermal energy. In contemporary applications, solar thermal catalytic techniques typically necessitate the use of solar concentrators to direct sunlight onto a receiver, where it is absorbed to produce high temperatures (exceeding 1000 K) in the material, thus facilitating catalytic reactions [31]. Solar thermal reactors can harness intense heat to promote endothermic chemical reactions, such as nitrogen fixation, methane dry reforming, CO₂ reduction, and converting CO₂ into synthesis gas or hydrocarbons [32–34]. Recently, there has been significant interest in photothermal chemistry that combines photochemical and thermochemical processes. For instance, Xiong group designed and synthesized a nonmetallic plasmonic catalyst MoN₂/MoO_{2-x} with photothermal unit and dual active sites unites for absorbed and activation of CO₂ as well as H₂, which exhibits excellent photothermal catalytic activity in reverse water-gas shift reaction. CO yield rate of 355 mmol·g_{cat}⁻¹·h⁻¹ with selectivity of 99% was achieved under illumination of full-spectrum light for 168 h with 3 W·cm⁻² [35]. Liu et al. reported single atom catalyst Ni/CeO₂ with solar-to-chemical efficiency of 1.14% and selectivity ~100% under concentrated light irradiation [36]. Innovatively, Feng et al. reported a Cu/Cu₂Se-Cu₂O heterojunction nanosheet array under visible–near-infrared light illumination. Ethanol producing rate and apparent quantum yield is 149.45 μmol·g⁻¹·h⁻¹ and 0.286% [37].

In the future, the photothermal effect is expected to be utilized more widely for various energy and environmental challenges, such as seawater desalination [38,39], water vaporization [40,41], air purification [42,43], wastewater treatment [39,41], and catalytic reduction of CO₂ to fuel [44]. There have been some reviews on the photothermal CO₂ transformation, which are out of the scope of this part. Next, we summarize the works of photothermal catalytic CO₂ cycloaddition as follows. This section presents the classification of catalyst materials based on their type, such as carbon materials, POM, MOFs, COF, ILs, and composite materials as shown in Table 2.

2.1. Carbon-Based Catalysts

Due to high aspect ratio, excellent mechanical, thermal and optical properties, carbon material could absorb full-spectrum light and transform the absorption photon to heat, which heat the catalyst to drive catalytic reaction inside. For example, carbon aerogels are used as seawater desalination, photothermal antibacterial materials and other applications [45]. Using carbon materials as photothermal catalysts to activate the loaded catalytic center can enable efficient direct solar-light-induced reactions without relying on external heat sources, while recent researchers have also pointed out that this catalytic mechanism is different from the traditional catalytic mechanism driven by external heat.

2.1.1. Heteroatom Doping Carbon Material

Various organic compounds can be thermally decomposed to produce carbon materials [46–48]. Due to its advantages such as metal and organic ligands, easily adjustable composition, and porous pore structure, MOFs materials have become the most promising precursors for the preparation of carbon material catalysts by pyrolysis method. Gao et al. utilized MOF-templated pyrolysis method to generate Br/N-co-doped carbon (Br-CN) for CO₂ cycloaddition. The remarkable catalytic performance of BN-CN-1-550 in the absence of cocatalysts and under full-spectrum light exposure can be primarily ascribed to its excellent photothermal conversion efficiency and the presence of numerous nucleophilic sites (Br ions) [49]. Wang et al. conducted a pyrolysis of a precursor made from phenylboronic acid, melamine, and ZIF-8 (Zeolitic Imidazolate Frameworks) to produce hollow mesoporous carbon co-doped with zinc, boron, and nitrogen (BHNC). The enhanced catalytic performance of the optimized BHNC under light and ambient conditions is due to its large specific surface area, hollow mesoporous architecture, improved light absorption capacity, and active sites for CO₂ chemical adsorption [50].

Besides MOFs, other organics precursors like natural products have also been explored as photothermal carbon-based catalyst for CO₂ cycloaddition reaction. Shan and Zhi et al. synthesized Zn, N-co-doped porous carbon (ZNCs) using glucose and melamine through a one-step pyrolysis process in a nitrogen atmosphere. The optimal sample, ZNC-800, features a layered structure with uniformly distributed Zn and N atoms, improved light absorption, and an impressive photothermal conversion efficiency of 51.3%. Hence, ZNC-800 achieved high yield of cyclic carbonate to 91.1% [51]. Yao group conducted much works focusing on carbon catalyst for photothermal catalytic CO₂ cycloaddition. They found that tea saponin, a biomass waste in the production of seed oil from camellia seeds, can be converted into porous saponin-derived carbon (CTS), which contains a large number of -OH and -COOH groups, exhibiting properties of Lewis acidic characteristic. The selectivity of epichlorohydrin carbonate in CO₂ cycloaddition reaction catalyzed by CTS-800 is 99% within 24 h [52]. In addition, Yao and Ding et al.

synthesized a photothermal catalyst N, B co-doped biochars (NB-BC) by doping corn stalk with B and C through one-step and two-step calcination. Due to the changes in pore structure, electronic structure, and active sites caused by doping of B and N, the catalytic performance was improved. Specifically, under visible light irradiation (400 mW/cm², 170 °C) for 26 h, the CO₂ cycloaddition yield was 99%, and the material still exhibited catalytic performance after 10 consecutive cycles, indicating good stability [53]. Venkataraman Mahalingam et al. also found that Cal-CS (calcined chitosan) photothermal catalysts formed by calcining biopolymer chitosan at different temperatures exhibit excellent photothermal conversion ability and catalytic activity for cycloaddition reaction of CO₂ and epoxides to produce cyclic carbonates [54].

However, although the light-induced thermal effect provided by carbon materials can effectively increase the reaction temperature, the strength of surface impurity atoms serving as Lewis acid/base sites still needs to be improved. Therefore, people have tried to further improve the catalytic reaction efficiency by intentionally adding metal atoms with stronger Lewis acidity during the synthesis of carbon materials, for example, single-atom catalysts based on carbon and composite materials with heterogeneous structures composed of carbon materials.

2.1.2. Carbon-Based Single Atom Catalysts (SACs)

Since the milestone work of Zhang et al. [55], single atom catalysis attracts extensive interests in CO₂ catalytic conversion. As shown in Figure 7, Jiang group firstly reported carbon-based Zn single atom catalyst with photothermal effect (metal amount up to 11.3 wt%) for CO₂ cycloaddition under light irradiation. They imaginatively adopt polystyrene (PS) nanospheres as hard template to construct hollow ZIF-8 precursor, which were thermally decomposed to obtain hollow porous carbon (HPC) supported with Zn SACs. The valence state of zinc atom is +2 and it exists in coordination with Zn-N₄, serving as a Lewis acid-base catalytic site in the reaction. The HPC-800 exhibits superior yield of 94% at atmospheric CO₂ under light irradiation for 10 h. Since then, Zinc-based metal sites have been implanted to various carbon supports to construct carbon-based photothermal CO₂ cycloaddition catalysts [56]. With the flourishing development of single atom catalysis, Yang and Liu et al. directly pyrolyzed nitrogen-rich MOFs to synthesize nitrogen doped carbon (Zn SA-NC) loaded with zinc single atoms. Zn SA-NC exhibits ultra-high light collection efficiency of >97% range from 250 to 2500 nm due to the unique multiple light reflection of hierarchical porous structure, which achieved as high as yield of 97% under full-spectrum illumination at 1 atm CO₂ without external heating. They proposed Zn-N₄ sites was catalytic active centers, photothermal effect as well as the photoelectron transfer may enhance adsorption as well as activation of inert CO₂ molecules [57].

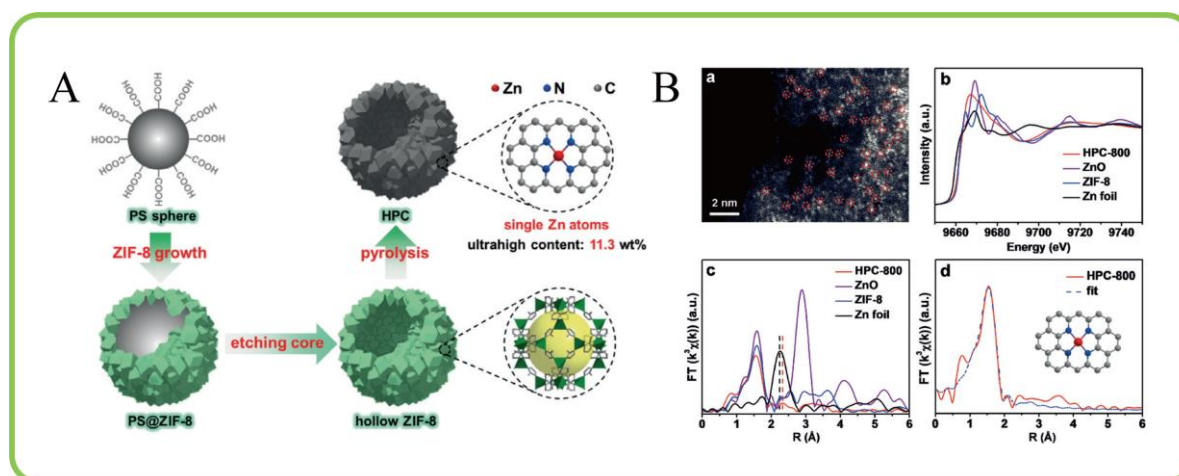


Figure 7. (A) Synthesizing route of HPC; (B) The SEM, TEM, and HAADF-STEM images of HPC-800; (a) HAADF-STEM image and corresponding (b–d) EXAFS information of HPC-800. Reprinted with permission from Ref. [56], Copyright 2019 Angewandte Chemie.

Besides characteristic Zn atom with superior Lewis acidity, other types of single atom like Tb and Al etc have also been investigated. Chen and Lu et al. synthesized an Al/N-Carbon single atom catalyst (14.4 wt%), which exhibited excellent catalytic performance for CO₂ cycloaddition reaction under light irradiation as shown in Figure 8 (95% conversion rate, 3.52 mmol·g⁻¹·h⁻¹). In addition to the efficient photothermal conversion, the transfer of photogenerated electrons from catalyst to reactants boosted the open-ring rate-determining step of epoxides [58].

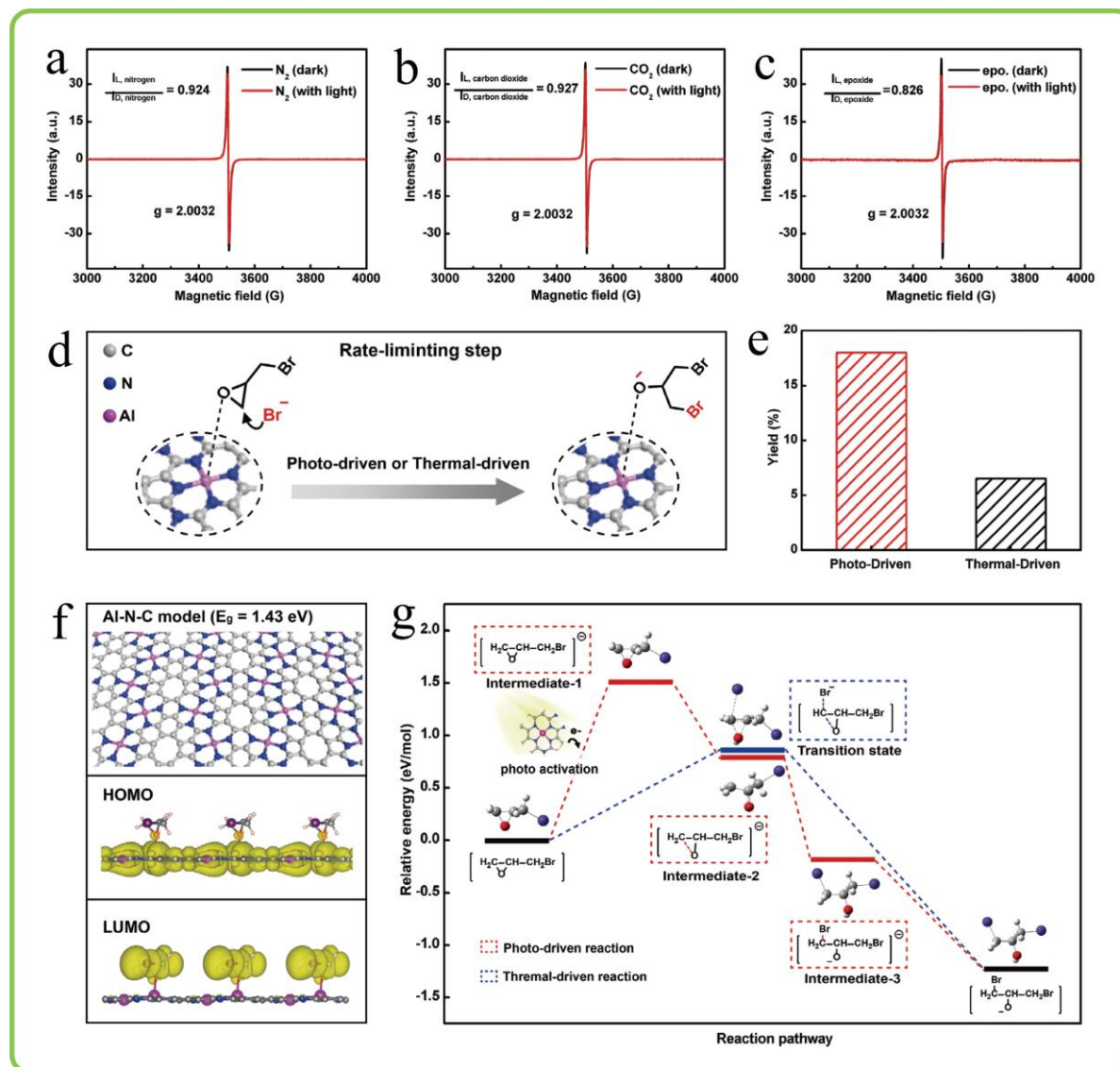


Figure 8. (a–c) EPR spectra of Al-N-C; (d) The rate-determining step of CO₂ cycloaddition with 1-bromo-2,3-epoxypropane; (e) Yield of ring-opening intermediates driven by heat and light, respectively; (f) HOMO-LUMO of Al-N-C with adsorption of 1-bromo-2,3-epoxypropane. (g) illustration of relative energy for the ring-opening of 1-bromo-2,3-epoxypropane under dark and illumination states. Reprinted with permission from Ref. [58], Copyright 2021 Advanced Materials.

2.1.3. Carbon-Based Composites Catalysts

In addition to single atom catalysts, some Zn-based composite have also been anchored on carbon substrates to drive CO₂ cycloaddition with photothermal effect. Dai and Yang et al. utilized zinc aspartate as a precursor to produce nanoporous N-doped carbon/ZnO. The resulting Zn-Asp-300 demonstrates a yield of 96.7% and nearly 100% selectivity at 80 °C when tetrabutylammonium bromide (TBAB) is used as a co-catalyst. Simultaneously, it also shows 92.2% of yield under visible and near-infrared light illumination. They asserted that ZnO, along with pyridinic and pyrrolic nitrogen atoms, functioned as Lewis acid and base sites, respectively, to collaboratively facilitate the CO₂ cycloaddition reaction [59]. Yao group synthesized ZnO/N-doped carbon with pyridinic N using Zn-ZIF-L as precursor by pyrolysis and oxidization treatment, which reached 76% yield of PC after 6 h with simulated sunlight of 120 mw/cm² (about 68 °C). It was revealed that well-dispersed ZnO nanoparticles, pyridinic N and surface oxygen groups were beneficial for the activation of epoxide, CO₂ and promotion of ring-opening step of epoxides shown in Figure 9A [60].

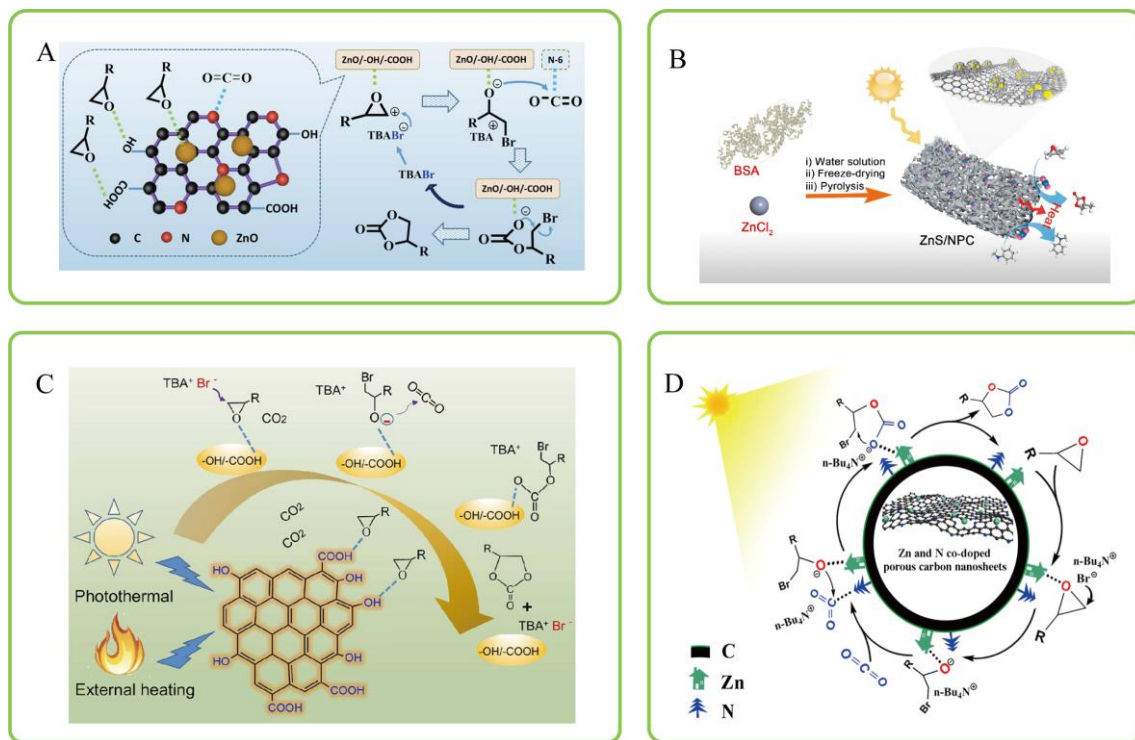


Figure 9. (A) Proposed reaction mechanism of CO₂ cycloaddition reaction on ZnO/NCO-L. Reprinted with permission from Ref. [60]; (B) Schematic illustration of synthesizing route of ZnS/NPC-X; Reprinted with permission from Ref. [61]; (C) Catalytic mechanism of CTS-800 for CO₂ cycloaddition reaction. Reprinted with permission from Ref. [52]. (D) Possible catalytic reaction mechanism of ZNCs. Reprinted with permission from Ref. [51]. Copyright Elsevier.

Besides ZnO, as shown in Figure 9B, other composites with superior surficial acid-basic properties have also been integrated with carbon to constructed photothermal catalysts. Niu et al. creatively used the Bovine serum albumin (BSA) to coordinate Zn cation to synthesize protein-Zn(II) networks, which was then converted to N-doped porous carbon-supported ZnS (ZnS/NPC-X) by pyrolysis under N₂ flow. The excellent catalytic performance for CO₂ cycloaddition under light illumination can be attributed to the hierarchical porous structure, high photothermal efficiency, and a wealth of Lewis acid/base sites. ZnS/NPC-2 achieves as high as yield of 98% and 89.6% under full-spectrum irradiation with 152.5 mW/cm² and natural sunlight, respectively (Figure 9C) [61]. Xu et al. prepared a photothermal catalyst of TbN₄B₂/C with B and Tb functionalized interconnected hollow carbon spheres via mesoporous SiO₂ high-temperature pyrolysis method. TEM and XAFS confirmed that Tb still existed in the form of a single atom. The Lewis acidity and valence state of Tb were enhanced by introducing of B element, which synergized with photoinduced charges to enhance ring-opening of epoxides and improve efficiency of photo-induced thermal-catalysis [62].

Based on the example given above, as the substrate of photothermal catalyst, carbon can enhance the absorption efficiency of light and convert it into heat energy. Doping other elements can further improve the efficiency of light adsorption and thermal conversion. Building on this, catalysts created by incorporating single atoms or other components onto carbon materials will enhance the Lewis acid and base sites, thus boosting the efficiency of CO₂ thermocatalytic epoxidation.

2.2. POMs (Polyoxometalates)

POMs, a class of metal oxide clustered anions, have received widespread attention in CO₂ photo-induced thermal-catalysis due to their structural diversity and specific electronic properties. The charges generated by photoexcited POMs can participate more effectively in the reaction with the assistance of heat. At the same time, the heat energy generated by adsorption light can promote the adsorption and activation of reactants, reduce the energy barrier of the reaction, and realize the synergistic effect of light and heat [63]. Recently, much efforts have been made to explore composite of POMs with semiconductors, metal nanoparticles, carbon materials, etc. For example, as shown in Figure 10, Peng first designed and synthesized phosphomolybdic acid modified ferrocene zirconium fluoride (PMO₁₂@Zr-Fc) metal organic frameworks (MOFs) nanosheets (PMO₁₂@Zr-FcMOFs). It showed an 88.05% yield of styrene carbonate under light intensity of 0.4 W/cm² for 8 h without additional heating.

The excellent catalytic activity of $\text{PMo}_{12}@Zr\text{-FcMOFs}$ was ascribed to the excellent photothermal properties of Lewis acidic of PMo_{12} and Zr-Fc MOFs nanosheets [64]. Niu et al. combined Keggin-type $[\text{BW}_{12}\text{O}_{40}]^{5-}$ polyoxometalates (POM) and amine catalysts to form a polymer based on naphthalimide (NDI) (CoW DPNDI PYI). The polymer demonstrates significant activity for the cycloaddition of CO_2 and epoxides under mild conditions (0.1 MPa CO_2 , $\leq 70^\circ\text{C}$) without the need for any cocatalysts, owing to the synergistic effects of Lewis bases at DPNDI and PYI sites, cobalt (II) Lewis acid sites, and POM Brønsted acid sites [65]. Wu et al. designed Co or Ce substituted POM cluster on GO with covalently grafted polyethyleneimine (PEI). The obtained POMs@GO-PEI exhibited local NIR photothermal effect, Lewis acid and base for CO_2 cycloaddition reaction. Under milder conditions, conversion of 98.9% for epoxide and selectivity of 99% for carbonate were achieved within 4 h, with a maximum TOF of 2718 h^{-1} [66]. Just recently in 2024, Wang et al. encapsulated PV_2W_{10} nucleophilic groups (Br^-) and PV_2W_{10} anions ($[\text{PV}_2\text{W}_{10}\text{O}_{40}]^{5-}$) in COFs nanocage due to electrostatic interactions. The obtained catalyst $\text{PV}_2\text{W}_{10}@EB\text{-TFP}$ solved the problem of lack of active sites in COF and simplified the reaction system. The catalyst $\text{PV}_2\text{W}_{10}@EB\text{-TFP}$ exhibited a large specific surface area and numerous dispersed active sites, leading to a conversion rate of 97.63% and selectivity of 100%. This work indicated that POM@COFs is a promising photothermal catalytic nanoreactor for CCR [67].

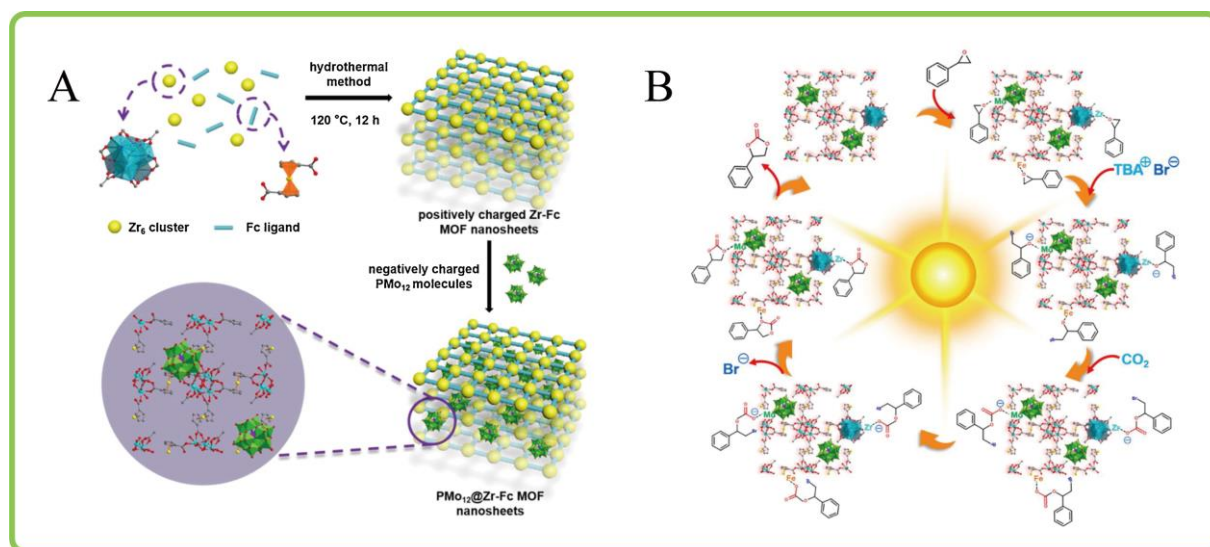


Figure 10. (A) Synthesis route of $\text{PMo}_{12}@Zr\text{-Fc MOF}$; (B) Reaction mechanism of CO_2 cycloaddition on $\text{PMo}_{12}@Zr\text{-Fc MOF}$. Reprinted with permission from Ref. [64], Copyright 2021 Elsevier.

2.3. MOFs (Metal Organic Frameworks)

Metal-organic frameworks (MOFs) are a type of porous material made up of metal-containing nodes and organic linkers. Their high porosity and tunable composition have led to their extensive application in areas such as small molecule screening, separation, catalysis, and adsorption [68–71]. Meanwhile, MOFs have always been regarded as excellent catalysts for CO_2 conversion, and many outstanding works have been done in thermal catalytic conversion of CO_2 by MOFs to synthesize carbonates [72–74]. Some excellent reviews have also been published [75–77], where we focus on the work of photothermal effects or photocatalytic cycloaddition reactions based on MOF materials.

Nagaraja et al. synthesized a 3D supramolecular Mn (II)-porphyrin MOF, which exhibited excellent catalytic activity with LED lamps under mild conditions with a 100% PO conversion. They proposed that the visible light absorption properties of porphyrin-Mn ligands generated superior catalytic activity, thereby enhancing the photothermal effect and promoting the activation of Mn(II) catalytic sites [78]. As shown in Figure 11A,B, Jiang et al. directly synthesized $\text{Co}_2\text{N}_{0.67}@ZIF\text{-67}$ by directly pyrolysis of ZIF-67, which showed superior activity compared to that of sole ZIF-67 for photocatalytic CO_2 cycloaddition with epichlorohydrin. This promotion is due to its high photothermal efficiency and effective activation of CO_2 [79]. Yao and Feng designed and prepared carbonized melamine sponge (CMS)@ MOFs (ZIF-8- NH_2 and MIL-88- NH_2). CMS featured a highly porous structure, a significant amount of nitrogen atoms, and excellent photothermal properties. In contrast, MIL-88- NH_2 (Figure 11C,D) and ZIF-8- NH_2 exhibited various acid-base characteristics. Therefore, a significant yield of 96% for cyclic carbonate at mild conditions was achieved for CMS@MOF. Wang et al. integrated $\text{Ti}_3\text{C}_2\text{T}_x\text{MXene}$ with bimetallic Zn/Fe ZIF through in-situ growth method to synthesize $\text{Zn}_{20}\text{Fe}_1\text{-ZIF/MXene}$. The interaction between

MOFs and MXene expanded the optical absorption range and effectively prevented the stacking of MXene. $Zn_{20}Fe_1$ -ZIF/MXene was subjected to epoxy chloropropane cycloaddition reaction and exhibiting enhanced activity (96% yield) (1 atm CO_2 , 350 mW/cm², 6 h) [80]. Yuan et al. fabricated a multicomponent MOF Zr-TFT-L1-L3 for efficient photothermal conversion of CO_2 to cyclic carbonates, which were ascribed to the Lewis acidic characteristic of Zr^{4+} sites, the nucleophilicity of iodide, and the photothermal property of tetrathiafulvalene (TTF)-naphthalene diimide (NDI) centers pairs [81]. Tu et al. prepared $Fe_2Co@BPDC$ with a spindle-shaped structure by introducing bimetallic and organic ligand BPDH. The experimental results indicated that the concentration of active sites and oxygen vacancies in the $Fe_2Co@BPDC$ catalyst increased, ultimately leading to a yield of cyclic carbonates as high as 92% under ultraviolet light irradiation at 70 °C and atmospheric pressure [82].

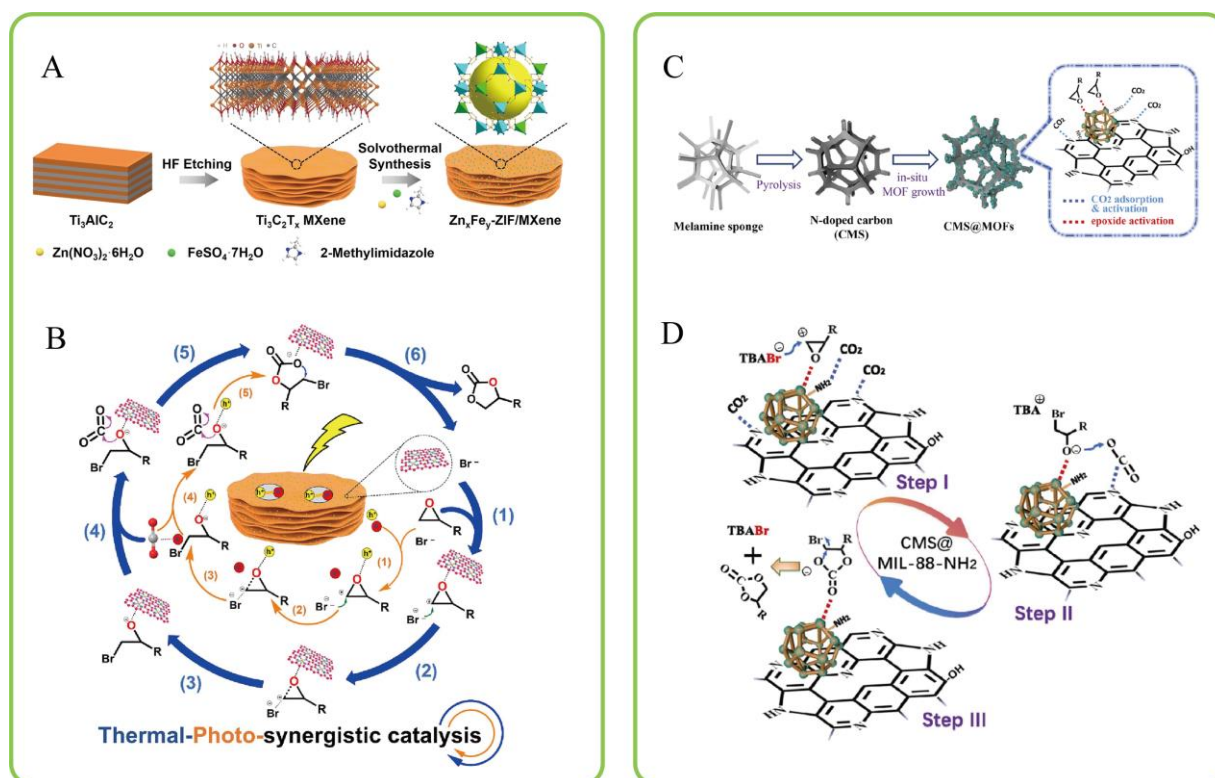


Figure 11. (A) Proposed reaction mechanism of CO_2 cycloaddition over $Zn_{20}Fe_1$ -ZIF/MXene; (B) Synthesis diagram of Zn_xFe_y -ZIF/MXene. Reprinted with permission from Ref. [80]; (C) Proposed catalytic mechanism of CO_2 cycloaddition on CMS@MIL-88-NH₂; (D) The synthesis process of CMS@MOFs. Reprinted with permission from Ref. [83], Copyright 2024 & 2022 Elsevier.

2.4. COFs (Covalent Organic Frameworks)

Covalent organic frameworks (COFs) are a newly developed category of porous organic crystalline materials that have garnered significant interest because of their promising applications in catalysis [84–86]. In addition, as shown in Figure 12, compared to MOF, their high thermal stability compared to MOF and controllable pore structure are more conducive to the diffusion and transport of CO_2 and epoxy compounds, making it easier for reactants to approach the catalytic active sites, thus enhancing the corresponding catalytic reaction rate. Dong et al. designed and synthesized a three-in-one catalyst COF-PI-2 consisting of metalloporphyrin, imidazolium ionic liquid, and quinoline. A yield of 99% for the cycloaddition reaction between epichlorohydrin and CO_2 was achieved under visible light irradiation, attributed to its photothermal conversion capability and selective CO_2 adsorption. To our knowledge, this makes COF-PI-2 the first instance of a photo-thermally driven CO_2 cycloaddition [87].

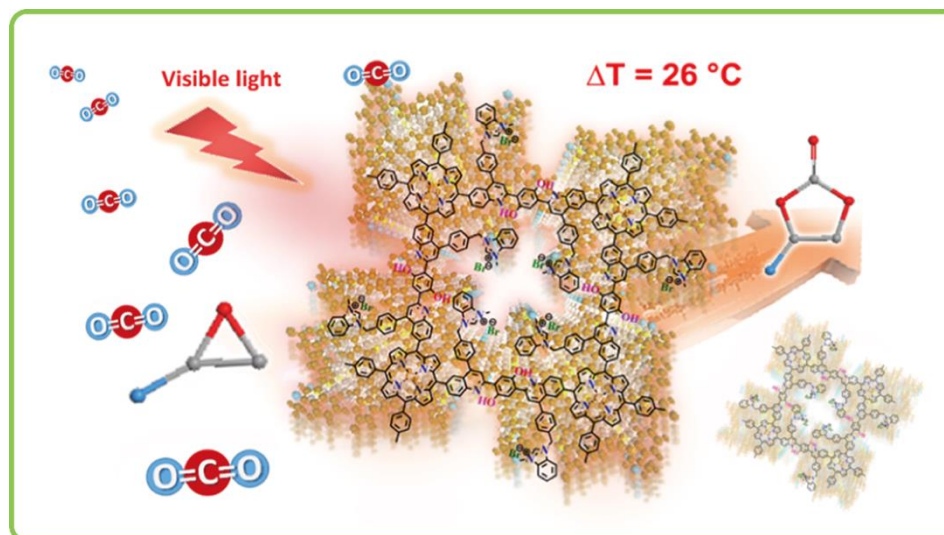


Figure 12. Schematic illustration of metalloporphyrin and ionic liquid-functionalized covalent organic frameworks COF-PI-2 for catalytic CO₂ cycloaddition. Reprinted with permission from Ref. [87], Copyright 2021 American Chemical Society.

2.5. ILs (Ionic Liquids)

Ionic liquids (ILs) are molten salts composed of large asymmetric organic cations and inorganic anions. ILs possess intrinsic properties such as excellent solubility and adsorption capacity, structural variety, non-flammability, a broad electrochemical window, and high ionic conductivity, which contribute to their extensive applications [88–90]. Imidazole ILs have been extensively developed to promote electrocatalytic CO₂ reduction as an attractive alternative to traditional electrolytes/solvents. The research interest in imidazole ILs mainly stems from their catalytic activity in activating CO₂, in addition to their excellent CO₂ adsorption capacity. Many related works emphasized the role of imidazole ILs as co catalysts. Jing et al. invented a method for preparing IL/Co-bCN nanocomposites by anchoring ILs and cobalt single atoms onto carbon nitride nanosheets. The optimized IL/Co-bCN nanocomposite exhibited nearly 100% CO selectivity for CO₂ reduction under UV–vis light irradiation. ILs extracted electrons and promoted CO₂ reduction, while cobalt single atoms captured holes and promoted water oxidation [91]. Zhang et al. developed a super crosslinked mesoporous poly(ionic liquids) combined with nickel-based bamboo-like nitrogen-doped carbon nanotubes (BNCNT) to create Ni-BNCNTs@HMPs-NH₂ for CO₂ cycloaddition. Ni-N-C sites, imidazole-derived poly (ionic liquids), carbon nanotubes, and plasma nickel nanoparticles functioned as Lewis acid sites, nucleophiles, and units for photothermal conversion, respectively. Most importantly, the photoexcited charges generated by the irradiation of Ni-N-C would promote rate limiting step of reaction (Figure 13) [92].

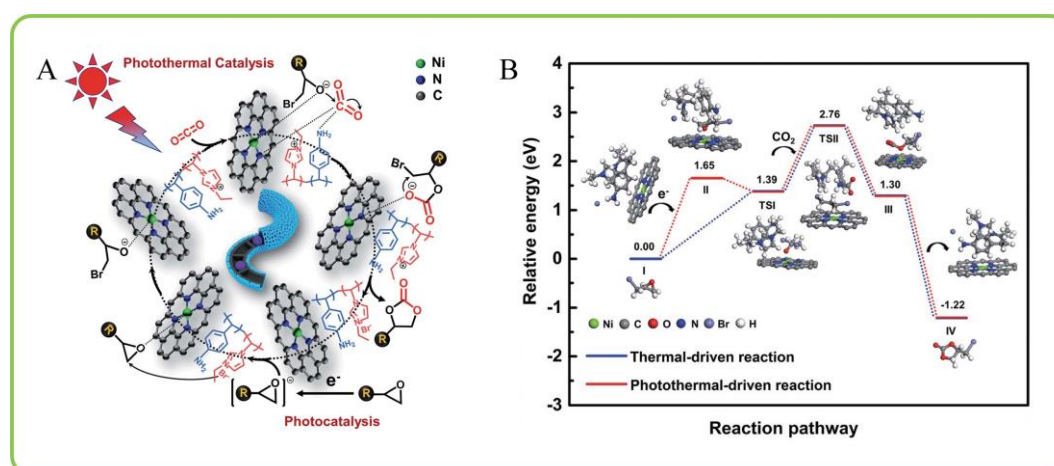


Figure 13. (A) Proposed mechanism of cycloaddition reaction between CO₂ and epoxide on Ni-BNCNTs@HMPs-NH₂; (B) Relative energy diagram for Ni-BNCNTs@HMPs-NH₂ under different conditions. Reprinted with permission from Ref. [92].

2.6. Other Photothermal Materials

In addition to works systematically discussed above, other excellent photo-to-thermal material induced by Localized surface plasmon resonance (LSPR) are also employed to utilize solar energy to drive cycloaddition of CO₂ with epoxide. Wu et al. successfully synthesized flower-shaped Co₂C for the first time, demonstrating remarkable catalytic performance in producing cyclic carbonates under blue LED ($\lambda = 450$ nm) irradiation, achieving yields as high as 95%. They proposed that, besides having outstanding photothermal conversion capabilities, the Lewis acid sites on the surface cobalt atoms could also activate CO₂ and epoxides, thereby improving the catalytic efficiency of CO₂ cycloaddition reactions (Figure 14A) [93]. Peng et al. developed CO₂-philic ferrocene-based porous organic polymers (Fc POPs) that achieved a cyclic carbonate yield of 94.7%. This was ascribed to the synergistic effect between Lewis acid-base interactions and intermolecular forces within the Fc POPs. It was worth noting that it even exhibited excellent performance in diluted CO₂ (15 vol%) with a yield of 93% (Figure 14B) [94].

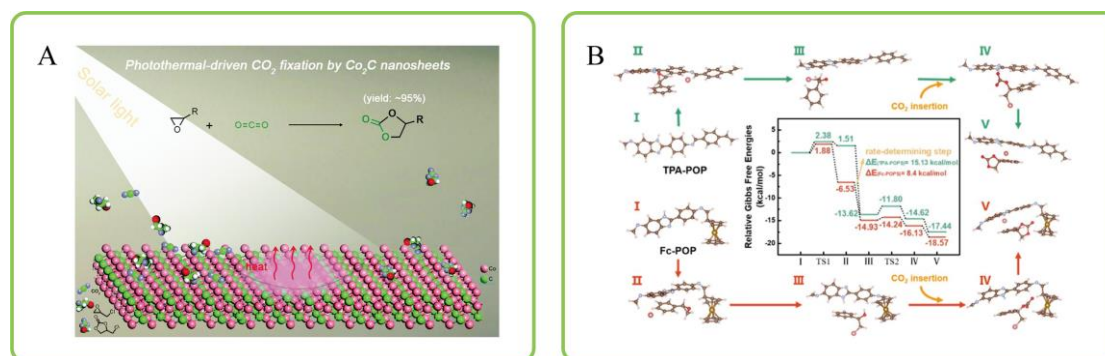


Figure 14. (A) Illustration of photothermal CO₂ cycloaddition reaction catalyzed by Co₂C. Reprinted with permission from Ref. [93]; (B) The energy profile diagram of Fc-POP (red) and TPAPOP (green) for CO₂ cycloaddition. Reprinted with permission from Ref. [94].

In summary, although photothermal conversion can drive CO₂ cycloaddition reactions without additional heat input, there are still some problems that need to be solved: On the one hand, the photothermal mode is more suitable for simple gas-solid-continuous reaction systems, while the CO₂ cycloaddition system is a gas-liquid-solid-intermittent multiphase reaction system. Some reactant molecules may have boiling points much higher than the photothermal temperature, and insufficient molecular thermal motion causes the epoxide molecules to not collide with the catalyst sufficiently to achieve the ideal ring-opening effect. On the other hand, the Kirchoff radiation law (the ratio of the energy emitted by a body at thermal equilibrium to the energy absorbed by it is independent of the properties of the body and only depends on the wavelength and temperature) shows that “hot” matter with a higher temperature has a greater heat loss efficiency, the photothermal effect of the catalyst alone cannot raise the temperature of the entire reaction system to the desired level. Furthermore, typical photothermal materials are concentrated on a few representative materials, which are not necessarily excellent CO₂ cycloaddition reaction catalysts. Light-heat conversion materials are introduced to raise the photothermal temperature, which interfere with the photochemical pathway (such as exciton-phonon coupling, deep potential wells, and non-radiative relaxation of photoelectrons).

Table 2. Summary of related literatures on photothermal catalytic CO₂ cycloaddition.

Entry	Type	Material	Cocatalyst	Light Source	Wavelength (nm)	Intensity	Temperature (°C)	Time (h)	Yield (%)	Conversion (%)	Reaction Rate	Ref.
1	Carbon-based	BHNC	TBAB		Full spectrum	300 mW·cm ⁻²		8	97			[50]
2		Carbonized tea saponins (CTS)	TBAB	UV-Vis light		350 mW·cm ⁻²	80	24	99.9	99		[52]
3		NB-BC	TBAB	Xenon lamp		400 mW·cm ⁻²		6	99			[53]
4		Cal-CS-300	TBAB	Xenon lamp		230 mW·cm ⁻²		6	97	92		[54]
5		HPC-800	TBAB	300 W Xe lamp	Full spectrum	300 mW·cm ⁻²	61	10	~94	96		[56]
6		Zn SA-NC	TBAB	Xenon lamp	Full spectrum	300 mW·cm ⁻²		16	97			[57]
7		Al-N ₄	TBAB	400 W Xe lamp	Full spectrum	400 mW·cm ⁻²	62		95		3.52 mmol·g ⁻¹ ·h ⁻¹	[58]
8		Zn-Asp-300	TBAB	Simulated sunlight	200–1100		80	4	92.2	96.3		[59]
9		ZnO/NCO-L	TBAB	Simulated sunlight		120 mW·cm ⁻²	RT	6	76			[60]
10		ZnS/N-Carbon	TBAB	300 W Xe lamp	Full spectrum	152.5 mW·cm ⁻²	65	12	98			[61]
11		TbN ₄ B ₂ /C	TBAB		380–1200	400 mW·cm ⁻²		6		87.9	739 mmol·g ⁻¹ ·h ⁻¹	[62]
12		ZNC-800	TBAB	300 W Xe lamp	Full spectrum	1000 mW·cm ⁻²	RT	10	93.3			[51]
13	POPs	PMO ₁₂ @Zr-Fc	TBAB	Simulated sunlight		400 mW·cm ⁻²	80	8	87			[64]
14		CoW-DPNDI-PYI		LED lamp			70	24	99			[65]
15		SiWCo@GO-PEI	TBAB	NIR light	808	1000 mW·cm ⁻²		4		98.9		[66]
16		PV ₂ W ₁₀ @EB-TFP	TBAB	LED lamp	350–780	540 mW·cm ⁻²	64	4	97.63			[67]
17	MOF	MOF1	TBAB	3×18 W				24		~100		[78]
18		CMS@MIL-88-NH ₂	TBAB	300 W Xenon lamp		350 mW·cm ⁻²	80	8	96			[83]
19		Co ₂ N _{0.67} @ZIF-67	TBAB	300 W Xe lamp		300 mW·cm ⁻²	66	3	95			[79]
20		Zn ₂₀ Fe ₁ -ZIF/MXene	TBAB	Xe lamp	Full spectrum	350 mW·cm ⁻²		6	96	96		[80]
21	COF	COF-P1-2	TBAB	500 W Xenon lamp	>400	80 mW·cm ⁻²	25	24	99			[87]
22	Ionic liquids	IL/Co-bCN		300 W Xe lamp			RT			20.6 μmol g ⁻¹ h ⁻¹		[91]
23		Ni-BNCNTs@HMPs-NH ₂		300 W Xe lamp		0.4 W·cm ⁻²		12	99			[92]
24	Other materials	Co ₂ C	TBAB	Blue LED	450	100 mW·cm ⁻²	60	15	93.5			[93]
25		Fc POPs	TBAB	Natural sunlight		0.3 W·cm ⁻²	88.7	8	94.7			[94]

3. Photocatalysis

Photocatalysis employs light energy to drive chemical reactions. The principle of photocatalysis is to use light energy to excite semiconductor photocatalysts, generating photogenerated electrons and holes. These electrons and holes can further undergo redox reactions with reactants, thereby achieving the process of converting light energy into chemical energy. So far, finding suitable and efficient catalysts remains the most critical step in research. Since 2018, there have been many articles on photocatalytic CO₂, which aim to achieve carbon neutrality through photocatalysis by designing different types/types of catalysts (Table 3) [95–98]. The primary processes in the photocatalytic synthesis of cyclic carbonates from CO₂ and epoxides involve photoexcited semiconductors and photocatalytic reactions. When photocatalysts are excited by light, photogenerated charge carriers separate to produce photogenerated electrons and holes. Electrons generated by light can activate CO₂, transforming it into CO₂ anions. At the same time, photoinduced holes function as Lewis acids to activate epoxides, making them more prone to nucleophilic attack and subsequent ring opening. Furthermore, the reaction intermediates after ring-opening undergo complete a closed loop reaction with CO₂ anions to obtain the corresponding product cyclic carbonate [99].

3.1. Single Atom Catalysts

As a Representative work, Tan et al. reported a two-dimensional (2D) monolayer ZnIn₂S₄ (ZIS) nanosheet composite material (Co-s-ZIS) modified with cobalt (Co) single atom (SA) and Co and Zn dual active centers immobilized with epoxides under visible light. By enhancing the presence of dual active functional groups and facilitating carrier separation, the interaction between epoxides and CO₂ was effectively adsorbed and stimulated. Furthermore, the energy barrier for CO₂ was further lowered due to the synergistic oxidation involving photoexcited electrons and holes. Experiments indicated that 2% Co-s-ZIS served as the most effective photocatalyst, achieving an epoxide conversion rate of 7.21 mmol·g⁻¹·h⁻¹, which is 3.5 times greater than that of the original ZIS, as illustrated in Figure 15A,B [100].

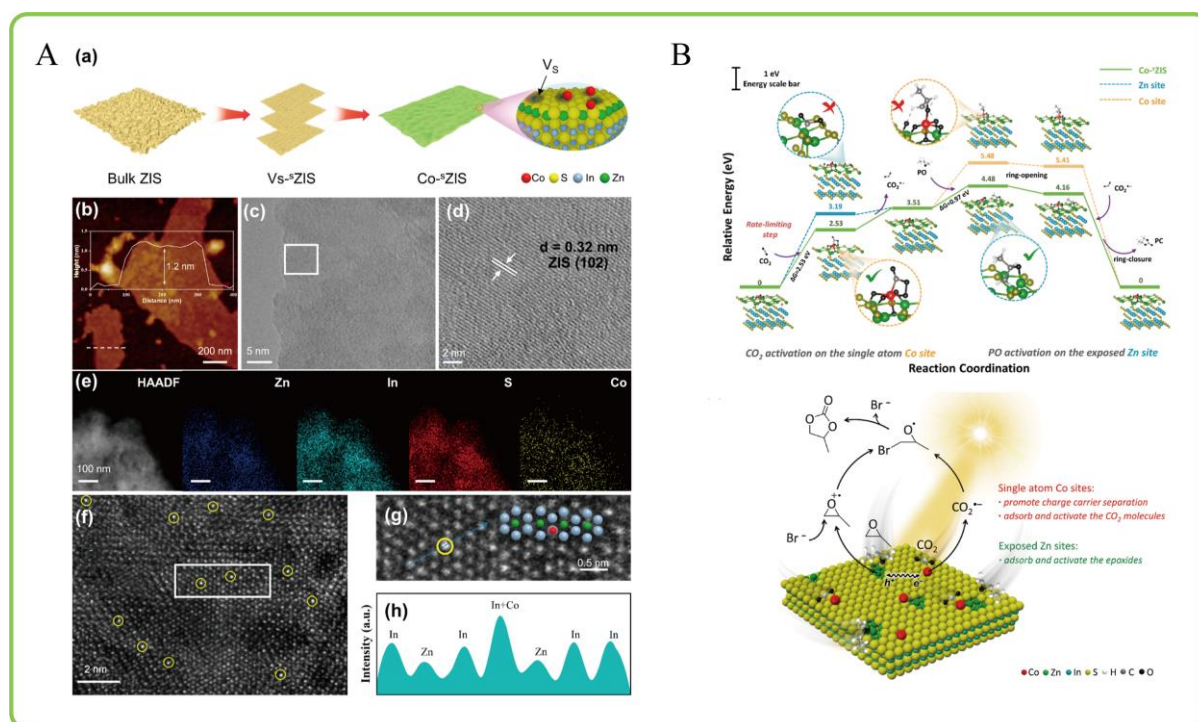


Figure 15. (A) (a) Synthesizing route of Co-s-ZIS. (b) AFM; (c,d) HRTEM; (e) HAADF-mapping images; (f-h) AC-HAADF-STEM images of Co-s-ZIS. (B) Diagrams of free energy and the suggested reaction mechanism for photocatalytic CO₂ cycloaddition on Co-s-ZIS are presented. Reprinted with permission from Ref. [100], Copyright 2023 American Chemical Society.

3.2. Heterostructural Composite

The first application of photocatalysis in CO₂ cycloaddition was published in 2018, when Suman Lata Jain et al. first attempted to synthesize cyclic carbonates with CO₂ and epoxides under visible light irradiation with

CoPc (cobalt phthalocyanine)/TiO₂ photocatalyst. Using a white cold LED as the light source ($\lambda > 400$ nm), the optimal CoPc/TiO₂ photocatalyst yield reached 94% at room temperature (RT) and 1atm CO₂ for 24 h. They proposed that the photo generated electrons of CoPc tended to reduce the absorbed CO₂ to $\cdot\text{CO}_2^-$, and the HOMO of CoPc accepted electrons from epoxides, which were converted into epoxide radical cations. Next, the steps of Br⁻ anion completed nucleophilic attack, PO ring opening, CO₂ insertion, and ring closure were completed, paving the way for photocatalytic CO₂ technology [101]. Ahmed Alzamly et al. further prepared BiNbO₄/r-GO visible light catalyst by hydrothermal method. When BiNbO₄/5% r-GO was used as the photocatalyst, the yield of 65% was achieved under visible light illumination. They believed that efficient suppress of charge carriers' recombination induced a large number of free radicals participating reaction [102].

In addition, as shown in Figure 16, carbon nitride (CN), as a star molecule, has attracted widespread research interest in photocatalytic CO₂ cycloaddition reactions due to its inherent semiconductor properties and easy adjustability. Huang et al. employed plasmon effect to design g-C₃N₄/Ag (ACN–Ag), which presented excellent activity of CO₂ cycloaddition. Amino-grafted ACN improved CO₂ chemisorption, and the transfer of photoexcited electrons from ACN to Ag generated high-energy electrons that activated propylene oxide [103]. Srivastava et al. prepared a Zr-thiamine modified carbon nitride (Zr-Thia/g-CN) catalyst through the pyrolysis of Zr-thiamine combined with urea. The Zr-Thia/g-CN catalyst showed good catalytic performance under traditional thermal catalysis as well as simulated light [104]. Tsiakaras et al. found W₁₈O₄₉/g-C₃N₄ exhibited PC yield up to 74% for CO₂ cycloaddition under AM 1.5 G irradiation. It was proposed that photoinduced electrons and Lewis acid-base sites were responsible for superior activity [105].

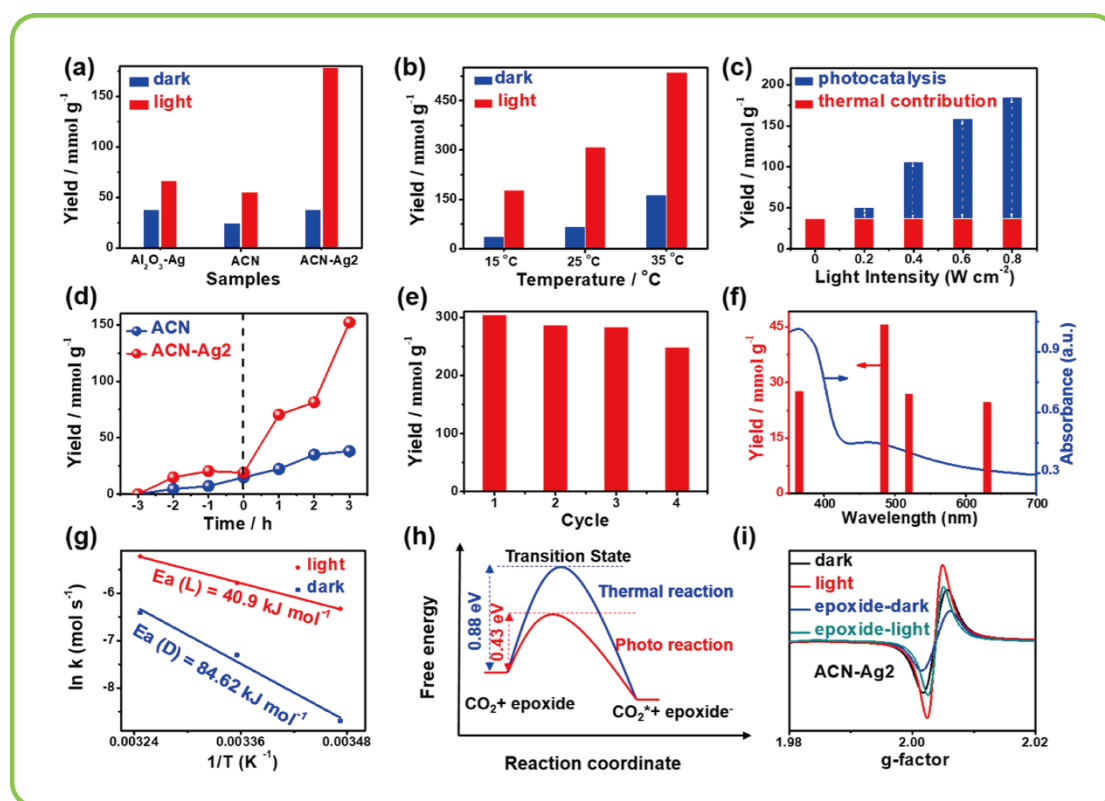


Figure 16. (a–d) Yield of PC under various reaction conditions; (e) Recycle stability of ACN-Ag2; (f) Yield under single wavelength light illumination; (g) E_a values; (h) Free energy diagram; (i) In situ EPR spectra of ACN–Ag2 under dark and light conditions. Reprinted with permission from Ref. [103], Copyright 2022 American Chemical Society.

Metal particles also have been found efficient for photocatalytic cycloaddition of CO₂. Gao et al. designed Pd nanoparticles implant on carbon vacancies of g-C₃N₄ nanotube to obtain Pd/SCNT500 catalyst, the enhanced CO₂ cycloaddition efficiency can be ascribed to unique morphology and optimized carbon vacancies based Pd coordination environment [106]. Pd and Pt nanoparticles have also been found useful for visible light-induced reaction by exploration of Pt/TiO₂/MWCNT and Pd/TiO₂/MWCNT photocatalysts. The catalytic activities were in sequence as follows: Pd/TiO₂/MWCNT > Pt/TiO₂/MWCNT > TiO₂/MWCNT > TiO₂ [107].

The rare earth metal compounds have also been found to exhibit excellent catalytic performance in photocatalytic CO₂ cycloaddition reactions. Alzamly et al. prepared BiLnO₃ (Ln = Sm, Eu, Tb, Er and Ho) by sol-

gel methods. They found that BiHoO₃ exhibited the highest epoxides conversion and yields of cyclic carbonate. Based on this, it is proposed to use lanthanide metal or bismuth as the Lewis acid nodes to break C-O bond of epoxide [108]. CeO₂ have also been explored as a photocatalyst. The S-scheme CdS–CeO₂ photocatalyst showed the highest yield of 96% and 99% selectivity of chloropropyl carbonate, respectively [109].

3.3. Metal Oxide Clusters

Crystalline metal oxide clusters (MOCs) represent a category of distinct molecular metal oxides, varying in size from small molecules to nanoparticles (NPs). They exhibit superior photocatalytic activity and Lewis acidity compared to traditional metal oxides, and can achieve outstanding catalytic active centers through meticulous control of their atomic structure. The titanium-oxide clusters (TOCs) attract academic attention due to its similarity to TiO₂ nanoparticles [110,111]. For example, by designing the composition, size, and surface structure of atomic clusters reasonably, adsorption and activation of CO₂ and epoxides can be improved, thereby promoting the progress of cycloaddition reactions. Wang group conducted much excellent work in this field. As shown in Figure 17A,B, Wang team developed and synthesized a Ti₁₈Bi₄O₂₉Bz₂₆ (where Bz stands for benzoate) cluster. Characterization results indicated that the S-scheme heterojunction created by the Ti₁₈O₂₂ and Bi₄O₇ components greatly enhanced the reduction capability of photo-generated electrons as well as the spatial separation of photo-generated carriers. Based on such merits, excellent cyclic carbonate yield was obtained by S-scheme Ti₁₈Bi₄O₂₉Bz₂₆ [112]. Guided by such idea, they continuously explored a series of titanium-oxide cluster photocatalysts for CO₂ cycloaddition, such as (H₃O)@Ti₇Cr₁₄ and Cs@Ti₇Cr₁₄ (Figure 17C,D) [113]. In addition, they designed five doped titanium-oxide cluster Ti₁₀M₂ (M = Cd, Pb, Ba, Sr, Ca), which showed catalytic activity in following order: Ti₁₀Cd₂ > Ti₁₀Pb₂ > Ti₁₀Ba₂ > Ti₁₀Sr₂ > Ti₁₀Ca₂ [114].

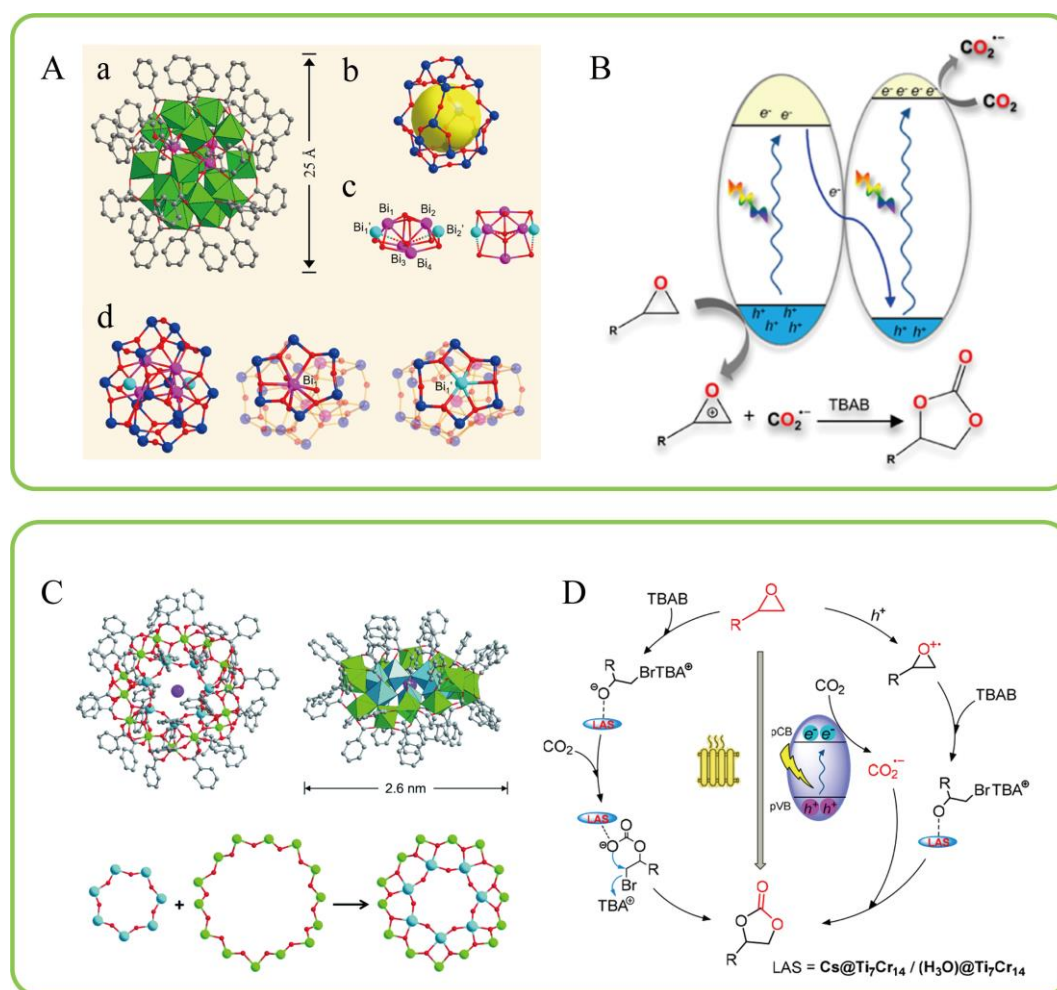


Figure 17. (A) (a) Ti₁₈Bi₄ model; (b) Ti₁₈O₂₆ host shell; (c) Bi₄O₇ cluster; (d) Ti₁₈O₂₆ shell stabilizing the Bi₄O₇ cluster; (B) proposed photocatalytic mechanism on Ti₁₈Bi₄; Reprinted with permission from Ref. [112]; (C) The top view and side view of Ti₇Cr₁₄ as well as its hierarchical illustration; (D) proposed photocatalytic mechanism on Cs@Ti₇Cr₁₄/(H₃O)@Ti₇Cr₁₄. Reprinted with permission from Ref. [113], Copyright 2022 American Chemical Society.

3.4. MOFs (Metal Organic Frameworks)

MOFs have the potential to serve as photocatalysts for CO₂ conversion because of their intrinsic porous structure and chemical makeup, along with a high specific surface area, significant CO₂ adsorption capacity, and adjustable active sites [86]. Significant efforts have been made to design various MOFs to drive cycloaddition reaction whether by photothermal we discussed above or sole photocatalysis discussed below. We will classify and summarized the sole photocatalysis of MOFs based on the types of core metal atoms.

(1) Ti MOF

Alzamly et al. chosen NH₂-MIL-125 (Ti) as a platform to synthesize BiNbO₄/NH₂-MIL-125 (Ti) and FeNbO₄/NH₂-MIL-125(Ti) photocatalysts, which exhibited good activity for photocatalytic CO₂ cycloaddition. The photogenerated electrons of Ti MOF tended to promote the oxidation-reduction of Ti (IV)-Ti (III), thereby inducing the single electron reduction of CO₂. The photogenerated holes were prone to adsorb epoxides and convert them into cations [115,116].

(2) Zn MOF

Lutakov and colleagues developed a heterostructured material composed of plasma-active copper nanoparticles and Zn Glu, demonstrating high efficiency in photocatalytic reactions involving various epoxides. They proposed that hot holes generated by plasma excitation could activate the epoxides that are adsorbed on the surface of Cu/ZnGlu [117].

(3) Ce MOF

M. Kirillov et al. synthesized cerium (III) MOF NH₂-Ce-MUM-2, which achieved yield of 99% for cyclic carbonate. The structure-activity relationship study showed that the acid-base characteristic, free amino in linker and Ce nodes contributed to the enhancement of performance [118]. Roy et al. compared CO₂ cycloaddition and CO₂ photoreduction catalytic reactions on Ce-BDC and Ce-BDC-NH₂, and concluded that Ce-BCC-NH₂ exhibited greater catalytic activity than Ce-BDC during the CO₂ fixation process because of the ideal quantity of Lewis acid sites provided by Ce³⁺ and Ce⁴⁺ [119].

(4) Fe MOF

Liu et al. synthesized a semi-amorphous Fe-BTC material that exhibits effective photocatalytic activity for the CO₂ cycloaddition reaction. They suggested that the electrons and holes generated by light excitation play roles in activating CO₂ and epoxides, respectively [120]. Huang and colleagues prepared two ferrocene-derived MOFs, Fe-FcDC and Al-FcDC. They suggested that the enhanced catalytic performance of Fe-FcDC was due to a longer metal-to-ligand-to-metal charge transfer (MLMCT) pathway and an extended carrier lifetime [121]. Zhang et al. developed a new two-dimensional porphyrin-based MOF, Fe-DBP(Co), demonstrating outstanding performance of 103.2 mmol·g⁻¹·h⁻¹. This phenomenon was ascribed to the movement of photoelectrons from CoDBP ligands to Fe clusters, coupled with the generation of Fe(II) and Co(III) resulting from the effects of electrons and holes, respectively [122].

(5) Mn MOF

Alzamly et al. developed a manganese-based MOF, UAEU-50, which attained a 90% yield of cyclic carbonates during photocatalytic CO₂ conversion under visible light illumination. They also suggested that the electrons generated by light excitation aided the cycloaddition reaction, while the photogenerated holes in UAEU-50 enhanced the ring-opening process of epoxides [123].

(6) Co MOF

Carrasco et al. prepared Hf/porphyrin-based metal-organic framework PCN-224 (M) (M=H, Co), which displayed the best performance for CO₂ cycloaddition reactions with epoxides. This performance can be linked to several factors, including structural stability, reduced cluster coordination, enhanced diffusion of reagents, and interactions with coordinatively unsaturated sites (CUS). Additionally, the greater oxophilicity of Hf⁴⁺ in the structure and the synergy between the Brønsted acid properties of the Hf⁴⁺ cluster and the Lewis acid characteristics of Co²⁺ also contribute to this effect [124].

Liang et al. synthesized layered columnar porphyrin-based metal-organic frameworks (Co-PMOFs) with a double-interpenetrated network structure. By combining photosensitive groups and regulating the structure, they exhibited high activity towards large-sized substrates. Under photocatalysis, most epoxides could be nearly 100% converted into cyclic carbonates within 6 h under mild conditions, and the materials had good stability [125].

(7) Zr MOF

Huang et al. introduced Zn or Ce into UiO-bpydc to obtain UiO-bpydc (M), where M = Zn or Ce. UiO-bpydc (Zn) displayed good performance for CO₂ cycloaddition. It was proposed that incorporating Zn not only effectively activated propylene oxide but also improved the ligand-to-metal charge transfer (LMCT) process [126]. Huang and Liu et al. incorporated a Lewis acid Bi atom into the porphyrin ring of MOF PCN-224 to create Bi-PCN-224. The LMCT process generated by light excitation promoted the electron transfer from Bi to Zr, followed by the reduced Zr⁴⁺ to Zr³⁺ subsequently. Such photophysical process activated CO₂ and photogenerated holes were beneficial to the epoxide ring-opening step [127]. Huang and Liu et al. created a boron-doped zirconium-based MOF, UiO-67-B, which showed improved light absorption and an enhanced ligand-to-metal charge transfer (LMCT) process when subjected to light irradiation. In addition, boron provided adsorption sites for CO₂ activation and avoided competition adsorption of epoxide on zirconium. Consequently, a notable yield of 372 μL of propylene carbonate can be achieved with UiO-67-B after 6 h of light exposure [128].

(8) Mg MOF

Xie et al. took Mg-MOF-74 to explore the mechanism of cycloaddition between CO₂ with epoxide. They showed that the photoinduced single-electron transfer from Mg-MOF-74 to CO₂ facilitated the formation of the ·CO₂⁻ radical, which was verified by in situ ESR spectroscopy results. Consequently, Mg-MOF-74 exhibited excellent photocatalytic performance (~97% yield) for CO₂ cycloaddition under ambient conditions (Figure 18) [129].

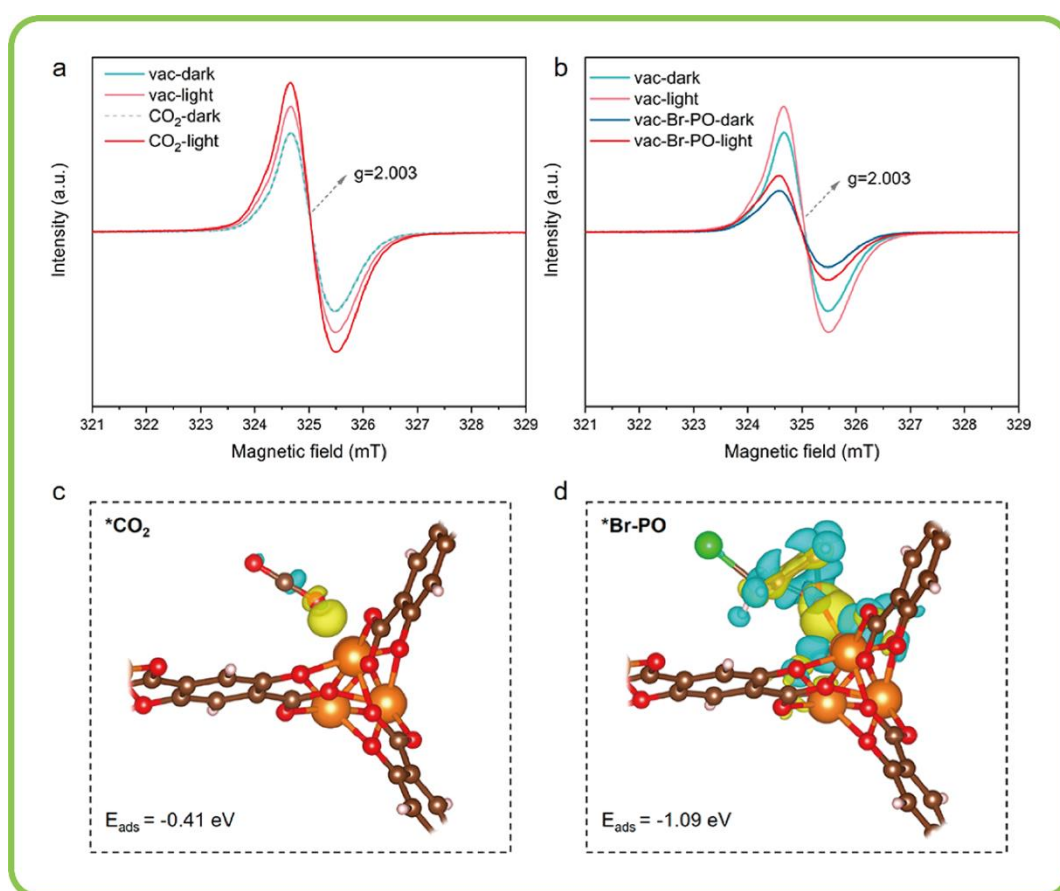


Figure 18. (a,b) In situ EPR of Mg-MOF-74 under CO₂ and PO atmosphere; (c,d) adsorption configuration and charge density difference of CO₂ and PO over Mg-MOF-74. Reprinted with permission from ref. [129], Copyright 2023 American Chemical Society.

(9) U MOF

Shi et al. introduced potassium ions to enhance framework interpenetration, which in turn increased the stability of the uranium-based porphyrin MOF IHEP-9, exhibiting remarkable thermal stability up to 400 °C. The IHEP-9 showed good catalytic activity for CO₂ cycloaddition under visible light illumination. They proposed photogenerated electrons and photogenerated hole activated CO₂ into free radical CO₂⁻ and promoted the epoxide converting into epoxide radical cation, respectively [130].

(10) In MOF

Zhai et al. incorporated a single vanadium site into the isostructural In-MOF to synthesize SNNU-97-InV. The significant CO₂ adsorption capacity and the broadened light absorption spectrum of SNNU-97-InV allowed it to effectively transform at least six types of epoxides into carbon compounds using CO₂. [131]. Zhang et al. fabricated amorphous MOF (NH₂-MIL-68), which achieved yield of 94.1% for styrene carbonate within 12 h for photochemical cycloaddition of CO₂ with styrene oxide. The open metal sites, hierarchically meso- and microporous structure and the increased carriers' separation efficiency of NH₂-MIL-68 were all beneficial for reaction [132].

(11) Cu MOF

Zhang et al. constructed a Cu-based MOF catalyst named CuTIA. Its large specific surface area and abundant acid-base sites enable it to serve as a bifunctional catalyst, exhibiting excellent performance in photocatalytic CO₂ reduction and cycloaddition reactions. It provides a new perspective for the design of highly efficient and selective MOF-based catalysts for CO₂ conversion [133].

3.5. COFs (Covalent Organic Frameworks)

Covalent organic frameworks (COFs) are a type of crystalline porous material featuring adjustable band gaps, extensive conjugated structures, and improved visible light absorption capabilities. These properties enable them to facilitate various photocatalytic reactions, including water splitting, nitrogen fixation, hydrogen peroxide synthesis, and organic synthesis, among others [134,135]. However, the limited number of building units, few active sites, and single-pore environment greatly restrict the efficiency of non-homogeneous catalytic reactions. Lei et al. attempted to prepare layered core-shell COFs with micro- and mesopores through rational structural design to improve the efficiency of non-homogeneous catalytic reactions. As shown in Figure 19, Lei et al. designed and synthesized a core-shell hierarchical pores material OH-P [5]-on-COF by “Macrocycle-on-COF” strategy with abundant of CO₂ adsorption sites. OH-P [5]-on-COF achieved conversion of 99% with the assistance of light within 3 h, exceeding previously reported COFs. Significantly, in this study COFs was used for photocatalytic cycloaddition of CO₂ for the first time. They demonstrated that the combined influence of photo-generated excitons, the multiple hydrogen bond effect, and bromide ions acting as nucleophiles facilitates the efficient progression of light-driven cycloaddition reactions under ambient conditions [136]. CTFs are a new type of COFs with good chemical and thermal stabilities. Zhang et al. designed a photocatalyst based on metalloporphyrin covalent triazine frameworks (Por-CTFs), which exhibits excellent catalytic performance for substrates with smaller groups [137].

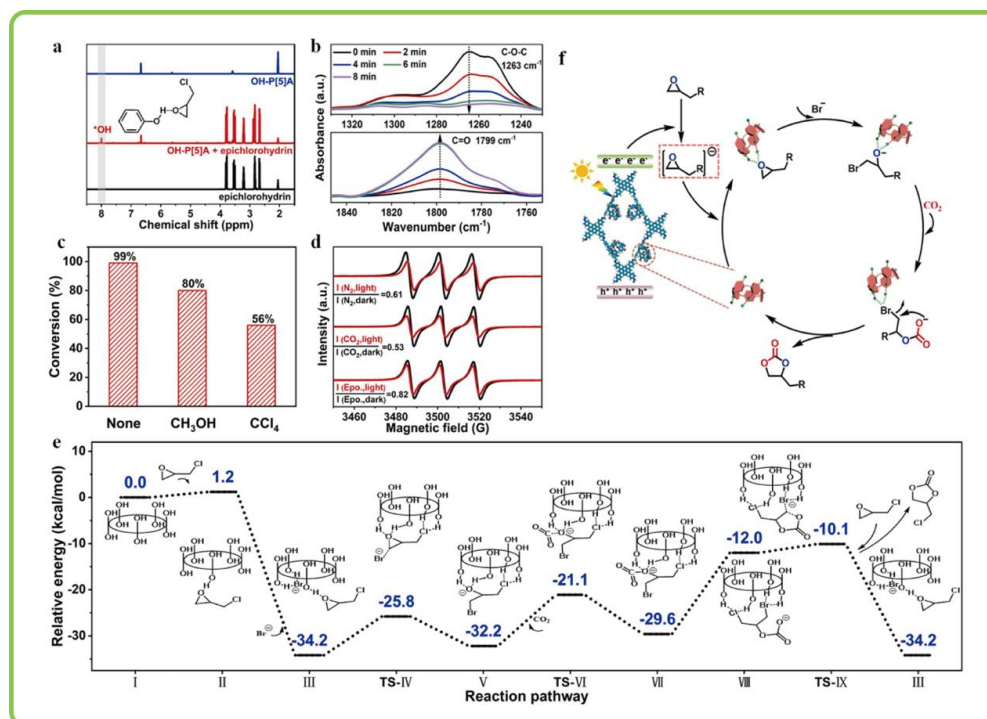


Figure 19. (a) ¹H NMR spectra of reactants and products; (b) in situ FT-IR spectrum; (c) Quenching experiments; (d) EPR spectra; (e) Energy profiles for the CO₂ cycloaddition reaction; (f) photocatalytic reaction mechanism on OH-P [5]. Reprinted with permission from ref. [136], Copyright 2024 American Chemical Society.

3.6. POPs (Porous Organic Polymers)

Porous organic polymers (POPs) are constructed by connecting various functional organic units through high-energy covalent bonds using a wide range of organic synthesis methods. POPs have recently emerged as a powerful species of heterogeneous photocatalysis. The structure of POPs is easily regulated due to the diverse construction units. Consequently, POPs represent an excellent option for CO₂ adsorption and catalytic conversion because of their large surface area, remarkable stability, and tunable chemical functional groups [94,138–140]. Mondal et al. designed conjugated Zn-metalated POP (Zn@MA-POP), which showed excellent performance in CO₂ cycloaddition reaction. The enhanced light absorption capacity, adjustable bandgap and the Zn core (ZnN₂O₄) active sites in Zn@MA-POP contributed to solar light-driven reaction shown in Figure 20 [141].

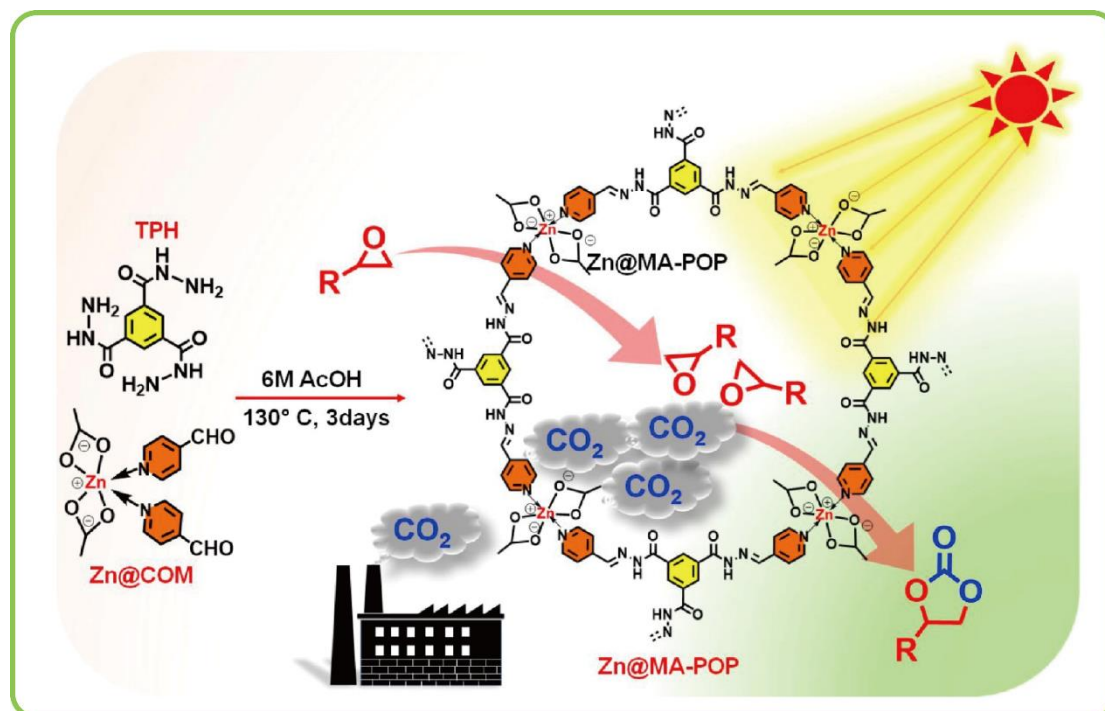


Figure 20. Schematic illustration of photocatalytic CO₂ cycloaddition on Zn@MA-POP catalyst. Reprinted with permission from ref. [141], Copyright 2022 American Chemical Society.

In summary, the above research results confirm that the photocatalytic mechanism promotes the ring-opening and CO₂ activation of epoxides in the photocatalytic pathway. Introducing a photocatalytic mechanism to regulate the reaction pathway is feasible. This brings new opportunities for CO₂ ring addition reactions under mild conditions. However, it should be noted that the limited improvement in catalytic reaction efficiency achieved by simply altering the reaction pathway through photocatalysis is currently not comparable to the efficiency of most thermal catalysis reactions [142].

Table 3. Summary of related literatures on photocatalytic CO₂ cycloaddition.

Entry	Type	Material	Cocatalyst	Light Source	Wavelength (nm)	Intensity	Temperature (°C)	Time (h)	Yield (%)	Conversion (%)	Reaction Rate	Ref.	
1	Single atom	Co-s-ZIS	TBAB	Visible light	>420		25	24	96.12		7.21 mmol·g ⁻¹ ·h ⁻¹	[100]	
2		Ga-C ₃ N ₄	TBAB	500 mW·cm ⁻²	365		65	12	>90			[143]	
3		CoPc/TiO ₂	TBAB	20 W LED	>400		25	24	94	96.7		[101]	
4	Composite	BiNbO ₄ /r-GO	TBAB	300 W Halogen lamp			80	24	65			[102]	
5		ACN-Ag	TBAB	300 W Xenon lamp	Full spectrum	0.6 W·cm ⁻²	15	6			177.6 mmol·g ⁻¹	[103]	
6		Zr-Thia/g-CN	DMAP	250 W Hg lamp			25	24		96		[104]	
7		W ₁₈ O ₄₉ /g-C ₃ N ₄	TBAB	300 W Xenon lamp			RT	4	74		271 mmol·g ⁻¹ ·h ⁻¹	[105]	
8		Pd/SCNT500	TBAB	Blue LED lamp	460	0.75 W·cm ⁻²		24			97	[106]	
9		Pd/TiO ₂ /MWCNT		LED lamp	>400		25	1	86–98			[107]	
10		BiHoO ₃	TBAB	400 W halogen lamp	340–850		RT	24			98	[108]	
11		CdS–CeO ₂	TBAB	300 W Xenon lamp			23–27	24	96			[109]	
12		Atomic Cluster	Ti ₁₈ Bi ₄ O ₂₉ Bz ₂₆	TBAB	300 W Xenon lamp			RT	14	>99	100		[112]
13			Cs@Ti ₇ Cr ₁₄	TBAB	Xe lamp			80	3	>99	100		[113]
14	Ti ₁₀ Cd ₂		TBAB	Visible light			80	1.5	>99	100		[114]	
15	BiNbO ₄ /NH ₂ -MIL-125 (Ti) _(50:50)		TBAB	300 W Halogen lamp			80	24	74			[115]	
16	FeNbO ₄ (75%)/NH ₂ -MIL-125(Ti) (25%)	TBAB	500 W Halogen lamp			75	72	52			[116]		
17	MOF	BioMOF	TBAB	LED	595	0.38 W·cm ⁻²	RT	24	81	86		[117]	
18		NH ₂ -Ce-MUM-2	TBAB				50	2	93			[118]	
19		Ce-BDC-NH ₂	TBAB				RT	48	97.1			[119]	
20		Fe-BTC	TBAB	30 W Blue LED	460		RT	6	90			[120]	
21		FeO ₆ MOF	TBAB	300 W Xe lamp				4	74.2			[121]	
22		Fe-DBP (Co)	TBAB	1000 W Xenon lamp	Full spectrum		RT	12		97.1		[122]	
23		UAEU-50	TBAB	400 W Halogen lamp			80	24	90			[123]	
24		PCN-224	TBAB				24	24	98			[124]	
25		UiO-bpydc (Zn)	TBAB	300 W xenon lamp			15	6			115 mmol·g ⁻¹	[126]	
26		Bi-PNC-224	TBAB	300 W Xenon lamp				6		99		[127]	
27		UIO-67-B	TBAB	Xenon lamp (300 W)	Full spectrum		RT	6			383 μL	[128]	
28		Mg-MOF-74	TBAB		Full spectrum		400 mW·cm ⁻²	60	12	97		[129]	
29		IHEP-9	TBAB	45 W, 6500 K compact fluorescent lamp	Visible light		RT	12	>99			[130]	
30	SNNU-97-InV	TBAB	300 W Xe lamp			25	24	73.3			[131]		
31	NH ₂ -MIL-68	TBAB	300 W Xenon lamp	380–780		25	12		99		[132]		
32	COF	OH-P [5]-on-COF	TBAB	LED lamp			20	3	99		[136]		
33	POPs	Zn@MA-POP	TBAB	250 W Xenon lamp			25	8	91		[141]		

4. Photo-Thermal Synergistic Catalysis

4.1. Reactions without External Heating

In recent years, the synergistic effects of photothermal and photocatalytic effects have been integrated to drive the cycloaddition reaction between CO₂ and epoxides. The key issue focuses on the design of dual active sites with photothermal units and photocatalytic units. Single-atom catalysts, MOFs and ZnIn₂S₄ can be used as photothermal synergistic materials with both photothermal response and photocatalytic activity. Zhang group synthesized the single-atom catalyst Ti-CNO by incorporating titanium into carbon and nitrogen co-doped carbon nanosheets, as illustrated in Figure 21. Under light irradiation and ambient pressure, the yield of styrene carbonate achieved with Ti-CNO reached 98.3%, significantly surpassing the yield obtained with the original CN, which was only 27.1%. The elevated photothermal effect induced by carbon nanosheets, along with the enhanced Lewis acidity/alkalinity, have a significant contribution to the catalytic activity. Further investigation confirmed that the Lewis acidic (Ti^{δ+}) sites and basic sites of Ti-CNO generated styrene oxide*⁺ and CO₂*⁻ under light irradiation, respectively, which served as crucial intermediates in the reaction process [144].

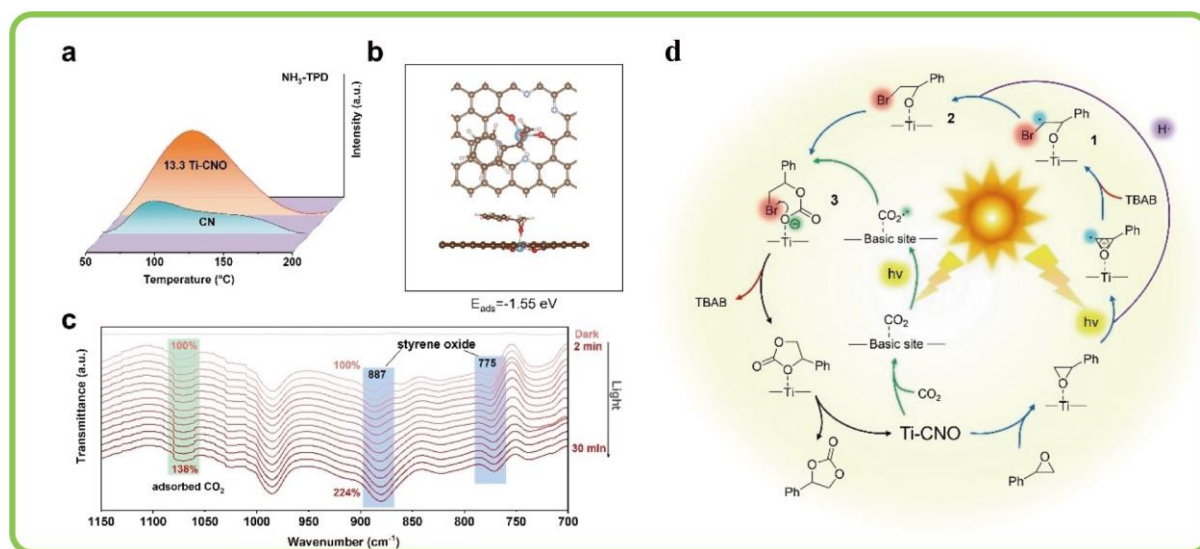


Figure 21. (a) NH₃-TPD; (b) The optimized SO adsorption configuration on 13.3 Ti-CNO; (c) In situ FTIR spectra of 13.3 Ti-CNO catalyst; (d) Possible catalytic mechanism of CO₂ cycloaddition on 13.3 Ti-CNO catalyst. Reprinted with permission from ref. [144], Copyright 2024 John Wiley and Sons.

Regarding MOFs, Huang et al. developed and synthesized a two-dimensional framework called FeTPyP, which demonstrated an impressive styrene carbonate yield of 106.13 mmol/(g·h) when exposed to light irradiation. In depth, they proposed that the superior catalytic activity was attributed to synergy between photocatalysis and thermal catalysis, which promoted the ring-opening of styrene oxide driven by ultraviolet light. Therefore, this work clearly demonstrates that the integration of thermal catalysis and photocatalysis offers a novel alternative strategy for designing efficient heterogeneous catalysts tailored for photo-induced CO₂ cycloaddition reactions [145]. Liu et al. synthesized Bi-HHTP MOF with a zigzagging corrugated topology, which demonstrated remarkable catalytic activity when irradiated with visible light. Furthermore, they proposed that the exposed Bi sites and photogenerated holes acted as Lewis sites for reactants and oxidation sites for epoxide. The synergistic effect of photocatalysis and photothermal effect promoted cycloaddition reaction [146].

Other novel composites like Zn ternary sulfide ZnIn₂S₄ have also been explored as photocatalytic photothermal catalyst for CO₂ cycloaddition. Zhang et al. developed a 2D/2D ZnIn₂S₄/Zn-NC-T S-scheme heterojunction composite using a low-temperature solvothermal technique. A cyclic carbonate yield of 98.8% was achieved after 4 h of full-spectrum illumination. This outstanding performance was ascribed to the efficient photothermal conversion enabled by the carbon matrix, along with the improved separation efficiency of photogenerated charge carriers due to the heterojunction structure. Consequently, it has been established that both photogenerated electrons and holes play significant roles in promoting the formation of ring-opening intermediates from epoxides and enhancing the polarization of adsorbed epoxides [147].

4.2. Reactions with External Heating

In other photothermal cocatalytic CO₂ cycloaddition reaction systems, both the photocatalytic effect of the material itself and the external applied thermal energy are required to jointly promote the reaction. This may be due to two considerations. On the one hand, separating light and heat will simplify the study of reaction mechanisms in catalytic reaction systems, enabling a better understanding of the roles and effects of light and heat in the reaction process [148–151]. On the other hand, the efficiency of thermal catalysis is significantly better than that of photocatalysis. Therefore, the combination of external thermal energy and photocatalytic mechanism can greatly improve the efficiency of photocatalysis and thermal catalysis.

For instances, Yang group prepared ZnIn₂S₄ nanosheets with highly exposed zinc sites (ZISe) (Figure 22A). They found that the ZISe catalyst achieved a conversion rate of 92.3% and selectivity greater than 99% for the cycloaddition of proepoxide (PO) with CO₂ when illuminated by blue LED light at a temperature of 80 °C. The specific roles of photogenerated carriers were confirmed. The photoinduced hole and electron promoted the coordination and polarization of adsorbed propylene oxide, leading to the creation of an electron-rich transition state for propylene oxide. This marks the inaugural report on the thermo-photo-synergistic catalytic cycloaddition of CO₂ using ZnIn₂S₄ [152]. Furthermore, as shown in Figure 22B, Yang et al. successfully produced Zn₃In₂S₆ containing sulfur vacancies (S_v), resulting in a 73.2% yield of cyclic carbonate at 80 °C when exposed to blue LED light for 2 h. Due to the improved dissociation of excitons and increased efficiency in separating photoinduced electron-hole pairs, electrons are likely to migrate to PO, resulting in an electron-rich state in the defective Zn₃In₂S₆-S_v. This process accelerated the rate-limiting step for CO₂ cycloaddition [153]. Zheng et al. employed a unique flower-like iron-based complex (Fe@NTC), which achieved a yield of up to 93% under UV light at 80 °C. The high activity was attributed to the presence of numerous active sites and excellent photothermal catalytic properties [154]. They also explored CoFe₂O₄@PDA, CoFe₂O₄@TPA catalyst in the same reaction and obtained the identical conclusion [155].

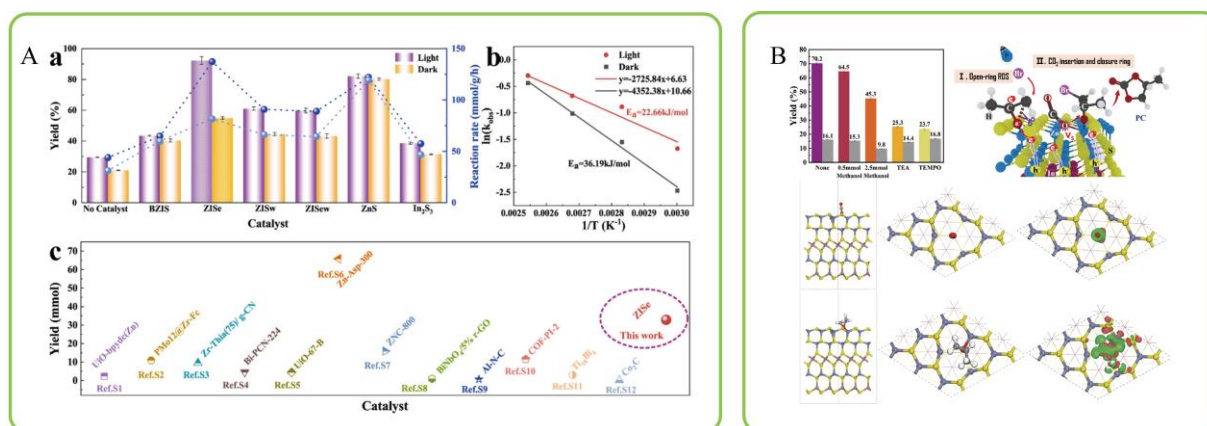


Figure 22. (A) (a) PC Yield of ZnIn₂S₄ and other catalysts for CO₂ cycloaddition. (b) Calculated E_a for ZISe under dark and light irradiation. (c) Performance comparison of ZISe and other reported catalyst. Reprinted with permission from Ref. [152]; (B) Catalytic mechanism of Zn₃In₂S₆-S_v towards CO₂ cycloaddition and adsorption behavior of PO, CO₂ over Zn₃In₂S₆-S_v. Reprinted with permission from Ref. [153], Copyright 2023 Elsevier & 2024 American Chemical Society.

In summary, the synergistic catalysis of light-thermal simultaneously uses the photocatalytic and thermal effects as driving forces to optimize the bottleneck steps of the ring addition reaction and improve the reaction rate from different perspectives: First, the reactant molecules absorb thermal energy to overcome the higher reaction activation energy, promoting the adsorption and desorption process of reactants and products. Second, the stability of excitons is easily affected by temperature, and when the system temperature is close to or greater than the exciton ionization energy, the exciton will decompose due to thermal excitation. The lattice thermal vibration optimizes the exciton dissociation kinetics and the photo-generated charge carrier transport kinetics, improving the exciton dissociation efficiency and the surface migration rate of photo-generated charge carrier. Third, thermal energy is more suitable for complex gas-liquid-solid-intermittent multiphase reaction systems from the perspective of reactant molecule collisions. Fourth, the “hot” charge carriers (electrons or holes) generated by exciton dissociation in the photochemical pathway have high energy, which migrate at high speed under thermal driving to the surface of the adsorbate’s LUMO to participate in the catalytic reaction. The efficiency of the ring addition reaction can be promoted by regulating the reaction pathway (Table 4).

Table 4. Summary of related literatures on photothermal synergistic catalytic CO₂ cycloaddition.

Entry	Type	Material	Cocatalyst	Light Source	Wavelength (nm)	Intensity	Temperature (°C)	Time (h)	Yield (%)	Conversion (%)	Reaction Rate	Ref.
1	No external heating	Ti-CNO	TBAB	300 W Xenon lamp	Full spectrum	2 W·cm ⁻²	88	6	98.3			[144]
2		FeTPyP	TBAB	300 W Xenon lamp	Full spectrum			5		92.1	530.67 mmol·g ⁻¹	[145]
3		Bi-HHTP	TBAB	300 W 18A Xenon lamp	>400	6.4 × 10 ³ W·cm ⁻²	62	3		>99	112 mmol·g ⁻¹ ·h ⁻¹	[146]
4	With external heating	ZIS/ZNC	TBAB	300 W Xenon lamp	Full spectrum		RT	4	98.8		82.3 mmol·g ⁻¹ ·h ⁻¹	[147]
5		ZISE	TBAB	Blue LED	446	100 mW·cm ⁻²	80	8	92.26			[152]
6		Zn ₃ In ₂ S ₆	TBAB	Blue LED	380	36 mW·cm ⁻²	80	2	73.2			[153]
7		Fe@NTC	TBAB	UV (250 W)			80	12	93			[154]
8		CoFe ₂ O ₄ @PDA	TBAB	250 W UV lamp	10–400		60	6	96			[156]

4.3. The Stability of Catalysts under Photo-Thermal Condition

Compared with the high temperatures in gas-solid photo-thermal catalytic reactions, the temperatures of most photo-thermal catalytic reactions in complex gas-solid-liquid three-phase systems such as CO₂ cycloaddition are below 100 degrees (Table 2). At such relatively low temperatures, the stability of the catalysts is mostly well maintained. Jiang et al. obtained the HPC-800 catalyst with Zn single-atom coordination by calcining hollow ZIF-8. Under the reaction conditions of 300 mW·cm⁻² full-spectrum light irradiation, a temperature of approximately 60 degrees was achieved. After three cycles of reaction, the authors characterized the bulk structure, micro-morphology, and Zn single-atom dispersion state of HPC-800 and found no changes in the catalyst, indicating excellent photo-thermal stability under these reaction conditions [56] (Figure 23A). Zhang and Rong et al. used the Ti single-atom catalyst 13.3 Ti-CNO loaded on CN to drive CO₂ cycloaddition under photo-thermal conditions, the reaction system reached an appropriate 88 degrees (2 W·cm⁻²). After 10 reaction cycles, no significant changes were observed in XRD, morphology, and elemental chemical environment [144] (Figure 23B). Most of the other photothermal catalysts (PV₂W₁₀@EB-TFP [67], Ni-BNCNTs@HMPs-NH₂ [92], PMo₁₂@Zr-Fc [64], and Bi-based MOF (Bi-HHTP) [146]) either maintained good photothermal structural stability.

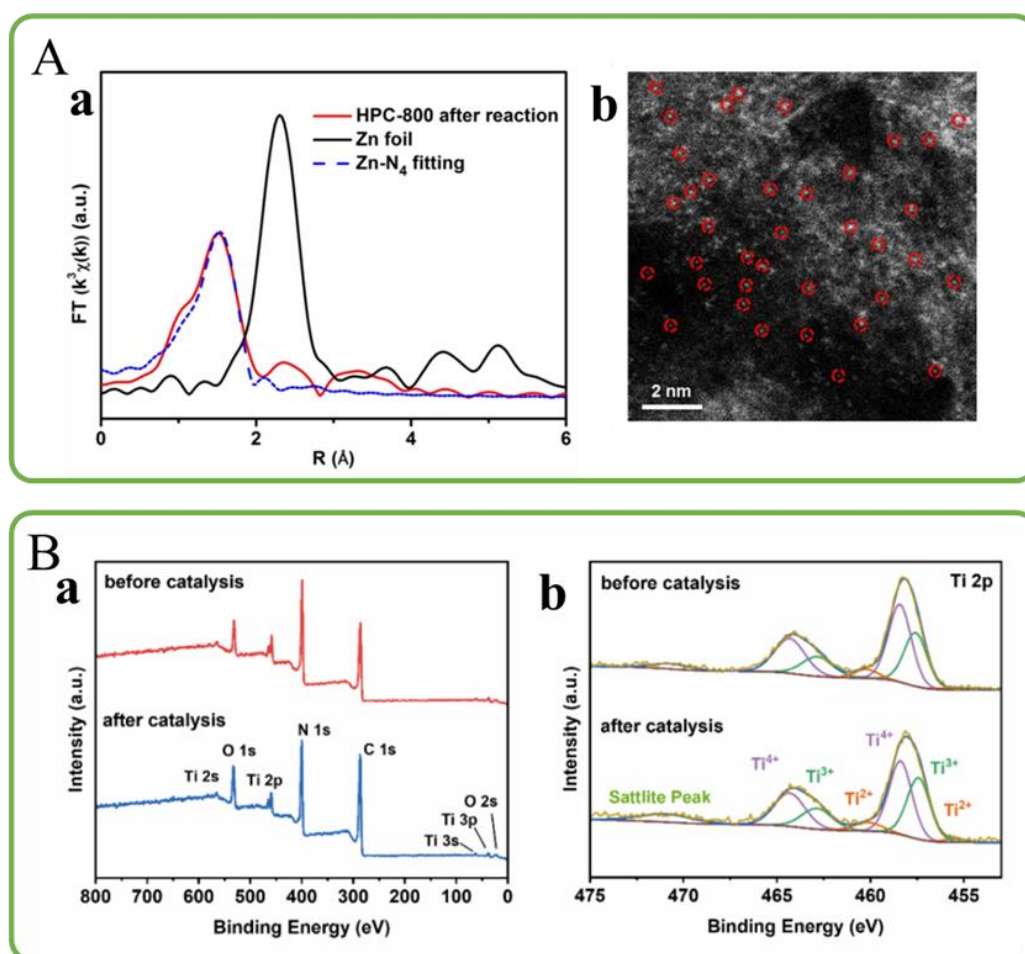


Figure 23. (A) (a) The k³-weighted Fourier transform (solid line) and the EXAFS R-space fitting curve (dotted line) of the EXAFS spectra of Zn foil and HPC-800 after three reaction runs. (b) The HAADF-STEM image of HPC-800 after three reaction runs. Reprinted with permission from Ref. [56]. (B) XPS analysis of 13.3 Ti-CNO: (a) survey spectrum and (b) Ti 2p spectrum, both before and after catalytic reactions. Reprinted with permission from Ref. [144].

5. Conclusion and Future Outlook

In summary, herein we summarized light-assisted CO₂ cycloaddition reaction from perspective of photo-induced thermal-catalysis, photocatalysis and photocatalysis&photo-thermal synergistic catalysis. Various advanced catalysts that can be driven by light, including single atom catalysts, MOFs, COFs and ILs etc. have been elucidated systematically. Despite rapid development and significant progress, there are still some unresolved issues that can be considered in future research in this field.

- (1) It is a mystery whether CO₂ can be reduced to its single electron reduction product CO₂^{·-} by photo generated charges;

In theory, the single electron reduction potential of CO₂ to CO₂^{·-} radical locates at -1.9 V vs. NHE, which is too negative to be achieved for potential of conduction band of common semiconductor. Therefore, some researcher insisted that CO₂ cannot be reduced to CO₂^{·-} during photo-(thermal)-catalytic in CO₂ cycloaddition reactions. On the contrary, some researchers have confirmed the presence of CO₂^{·-} intermediate by advanced in-situ technology, such as DRIFTS and EPR etc. Therefore, in the following research, it is suggested to clarify this dilemma to guide the in-depth exploration of catalytic mechanism.

- (2) The specific rate-determining steps in the photo-(thermal)-catalytic CO₂ cycloaddition reaction remain unclear.

The open-ring step of epoxide is rate-determining-step (RDS) in classical thermalcatalysis of CO₂ cycloaddition. However, photoinduced carries tend to activate epoxide and CO₂, and the RDS of light-assist reaction maybe different from thermalcatalysis. Therefore, in following research it should pay much attention to the clarify the clear catalytic mechanism and figure out the exact intermediates.

- (3) The roles of photogenerated electron and hole photo-(thermal)-catalytic CO₂ cycloaddition reaction needs to be clarified.

In photocatalysis, the photogenerated electron and hole act as reduction and oxidation sites, respectively. Some researchers proposed that photoinduced holes and electron tend to activate epoxide and CO₂, respectively. While other researchers found that photoinduced electron tend to activate both epoxide and electron. Thus, the roles of photogenerated electron and hole should be clarified in further research.

- (4) The yield of cyclic carbonate in photocatalysis should be improved largely.

Furthermore, the current yield of synthesizing cyclic carbonates through photocatalytic reactions is extremely low, far lower than traditional thermal catalytic pathways. Therefore, in the future research work, external thermal energy should be combined with photocatalysis to achieve satisfactory and industrial grade yields. The development of corresponding new catalytic reactors is also urgently needed.

Author Contributions: Writing-original draft, investigation, methodology, software, B.Z.; visualization, investigation, Q.C.; methodology, investigation; X.D.; supervision, funding, writing-reviewing and editing, X.Y. All authors have read and agreed to the published version of the manuscript.

Funding: This work received funding from Natural Science Foundation of Qingdao Municipality, China (23-2-1-226-zyyd-jch); Natural Science Foundation of Shandong Province, China (ZR2023ME094, ZR2021QB022, ZR2023QD095); National Natural Science Foundation of China (52172093, 52102362, 52301400).

Institutional Review Board Statement: Not applicable.

Informed Consent Statement: Not applicable.

Data Availability Statement: Not applicable.

Conflicts of Interest: The authors declare no conflict of interest.

References

1. Meinshausen, M.; Meinshausen, N.; Hare, W.; Raper, S.C.; Frieler, K.; Knutti, R.; Frame, D.J.; Allen, M.R. Greenhouse-gas emission targets for limiting global warming to 2 °C *Nature* **2009**, *458*, 1158–1162.
2. Vermeer, M.; Rahmstorf, S. Global sea level linked to global temperature. *Proc. Natl. Acad. Sci. USA* **2009**, *106*, 21527–21532.
3. Li, X.; Yu, J.; Jaroniec, M.; Chen, X. Cocatalysts for Selective Photoreduction of CO₂ into Solar Fuels. *Chem. Rev.* **2019**, *119*, 3962–4179.
4. Li, W.-L.; Shuai, Q.; Yu, J. Recent Advances of Carbon Capture in Metal-Organic Frameworks: A Comprehensive Review. *Small* **2024**, *20*, 2402783.
5. Gu, Y.; Wang, G.; Chen, X.; Xu, X.; Liu, Y.; Yang, J.; Zhang, D. Unlocking the Potential of CO₂ Capture: A Synergistic Hybridization Strategy for Polymeric Hydrogels with Tunable Physicochemical Properties. *Small* **2024**, *20*, 2402529.
6. Yang, D.; Li, S.; He, S.; Zheng, Y. Can conversion of CO₂ into fuels via electrochemical or thermochemical reduction be energy efficient and reduce emissions? *Energy Convers. Manag.* **2022**, *273*, 116425.
7. Jiang, M.; Wang, H.; Zhu, M.; Luo, X.; He, Y.; Wang, M.; Wu, C.; Zhang, L.; Li, X.; Liao, X. Review on strategies for improving the added value and expanding the scope of CO₂ electroreduction products. *Chem. Soc. Rev.* **2024**, *53*, 5149–5189.
8. Sakakura, T.; Choi, J.-C.; Yasuda, H. Transformation of the greenhouse gas carbon dioxide to graphene. *J. CO₂ Util.*

- 2007, 107, 2365–2387.
9. Mikkelsen, M.; Jørgensen, M.; Krebs, F.C. The teraton challenge. A review of fixation and transformation of carbon dioxide. *Energy Environ. Sci.* **2010**, *3*, 43–81.
 10. Xie, S.; Ma, W.; Wu, X.; Zhang, H.; Zhang, Q.; Wang, Y.; Wang, Y. Photocatalytic and electrocatalytic transformations of C1 molecules involving C-C coupling. *Energy Environ. Sci.* **2021**, *14*, 37–89.
 11. Meng, Q.-Y.; Wang, S.; Huff, G.S.; König, B. Ligand-controlled regioselective hydrocarboxylation of styrenes with CO₂ by combining visible light and nickel catalysis. *J. Am. Chem. Soc.* **2018**, *140*, 3198–3201.
 12. Chen, Y.; Li, M.; Li, Z.; Liu, F.; Song, G.; Kawi, S. Efficient syngas production via CO₂ reforming and electroreduction reactions through catalyst design. *Energ. Convers. Manag.* **2022**, *265*, 115744.
 13. Boot-Handford, M.E.; Abanades, J.C.; Anthony, E.J.; Blunt, M.J.; Brandani, S.; Mac Dowell, N.; Fernández, J.R.; Ferrari, M.-C.; Gross, R.; Hallett, J.P.; et al. Carbon capture and storage update. *Energy Environ. Sci.* **2014**, *7*, 130–189.
 14. Shaikh, R.R.; Pornpraprom, S.; D’Elia, V. Catalytic Strategies for the Cycloaddition of Pure, Diluted, and Waste CO₂ to Epoxides under Ambient Conditions. *ACS Catal.* **2017**, *8*, 419–450.
 15. Han, Z.; Rong, L.; Wu, J.; Zhang, L.; Wang, Z.; Ding, K. Catalytic Hydrogenation of Cyclic Carbonates: A Practical Approach from CO₂ and Epoxides to Methanol and Diols. *Angew. Chem. Int. Ed.* **2012**, *51*, 13041–13045.
 16. Fukuoka, S.; Kawamura, M.; Komiya, K.; Tojo, M.; Hachiya, H.; Hasegawa, K.; Aminaka, M.; Okamoto, H.; Fukawa, I.; Konno, S. A novel non-phosgene polycarbonate production process using by-product CO₂ as starting material. *Green. Chem.* **2003**, *5*, 497–507.
 17. Mishra, V.; Peter, S. A comprehensive overview on catalytic pathway for CO₂ utilization with epoxide to cyclic carbonate. *Chem. Catal.* **2023**, *4*, 100796.
 18. Darensbourg, D.J.; Yarbrough, J.C.; Ortiz, C.; Fang, C.C. Comparative kinetic studies of the copolymerization of cyclohexene oxide and propylene oxide with carbon dioxide in the presence of chromium salen derivatives. In situ FTIR measurements of copolymer vs cyclic carbonate production. *J. Am. Chem. Soc.* **2003**, *125*, 7586–7591.
 19. Darensbourg, D.J.; Yeung, A.D. A concise review of computational studies of the carbon dioxide-epoxide copolymerization reactions. *Polym. Chem.* **2014**, *5*, 3949–3962.
 20. Rao, R.; Ma, S.; Gao, B.; Bi, F.; Chen, Y.; Yang, Y.; Liu, N.; Wu, M.; Zhang, X.; Science, I. Recent advances of metal-organic framework-based and derivative materials in the heterogeneous catalytic removal of volatile organic compounds. *J. Colloid. Interf. Sci.* **2023**, *636*, 55–72.
 21. Taddei, M. When defects turn into virtues: The curious case of zirconium-based metal-organic frameworks. *Coord. Chem. Rev.* **2017**, *343*, 1–24.
 22. Samaniyan, M.; Mirzaei, M.; Khajavian, R.; Eshtiagh-Hosseini, H.; Streb, C. Heterogeneous catalysis by polyoxometalates in metal-organic frameworks. *ACS Catal.* **2019**, *9*, 10174–10191.
 23. Lin, X.; Zhang, M.; Lv, W.; Li, J.; Huang, R.; Wang, Y. Engineering Carbon Nanotube-Based Photoactive COF to Synergistically Arm a Multifunctional Antibacterial Hydrogel. *Adv. Funct. Mater.* **2024**, *34*, 2310845.
 24. Shan, T.; Luo, H.; Wu, S.; Li, J.; Zhang, F.; Xiao, H.; Huang, L.; Chen, L. In situ formation of a covalent organic framework on g-C₃N₄ encapsulated with nanocellulosic carbon for enhanced photocatalytic N₂-to-NH₃ conversion. *Fuel.* **2024**, *358*, 130157.
 25. Li, G.; Yue, Q.; Fu, P.; Wang, K.; Zhou, Y.; Wang, J. Ionic dye based covalent organic frameworks for photothermal water evaporation. *Adv. Funct. Mater.* **2023**, *33*, 2213810.
 26. Ejaz, M.; Mohamed, M.G.; Kuo, S.-W. Solid state chemical transformation provides a fully benzoxazine-linked porous organic polymer displaying enhanced CO₂ capture and supercapacitor performance. *Polym. Chem.* **2023**, *14*, 2494–2509.
 27. Su, X.; Yang, X.-F.; Huang, Y.; Liu, B.; Zhang, T. Single-atom catalysis toward efficient CO₂ conversion to CO and formate products. *Acc. Chem. Res.* **2018**, *52*, 656–664.
 28. Shan, P.; Ye, H.; Qian, B.; Zheng, Y.; Xiao, G. Boosting the catalytic activity of high-order Ruddlesden-Popper perovskite SrEu₂Fe₂O_{7-δ} air electrode by A-site La doping for CO₂ electrolysis in solid oxide electrolysis cells. *Fuel* **2024**, *367*, 131507.
 29. Feric, T.G.; Hamilton, S.T.; Ko, B.H.; Lee, G.A.; Verma, S.; Jiao, F.; Park, A.H.A. Highly tunable syngas product ratios enabled by novel nanoscale hybrid electrolytes designed for combined CO₂ capture and electrochemical conversion. *Adv. Funct. Mater.* **2023**, *33*, 2210017.
 30. Hong, Y.H.; Lee, Y.-M.; Nam, W.; Fukuzumi, S. Multi-functional photocatalytic systems for solar fuel production. *J. Mater. Chem. A* **2023**, *11*, 14614–14629.
 31. Ghossoub, M.; Xia, M.; Duchesne, P.N.; Segal, D.; Ozin, G. Principles of photothermal gas-phase heterogeneous CO₂ catalysis. *Energy Environ. Sci.* **2019**, *12*, 1122–1142.
 32. Moretti, C.; Patil, V.; Falter, C.; Geissbühler, L.; Patt, A.; Steinfeld, A. Technical, economic and environmental analysis of solar thermochemical production of drop-in fuels. *Sci. Total Environ.* **2023**, *901*, 166005.
 33. Giacoppo, G.; Trocino, S.; Lo Vecchio, C.; Baglio, V.; Díez-García, M.I.; Aricò, A.S.; Barbera, O. Numerical 3D model of a novel photoelectrolysis tandem cell with solid electrolyte for green hydrogen production. *Energies.* **2023**, *16*, 1953.

34. Yao, S.; Okumoto, M.; Madokoro, K.; Shimogami, J.; Suzuki, E.; Yashima, T. Plasma conversion of methane and CO₂ using a tubular circle-to-plate reactor. *J. Chem. Eng. Jpn.* **2003**, *36*, 435–440.
35. Wan, X.; Li, Y.; Chen, Y.; Ma, J.; Liu, Y.-A.; Zhao, E.-D.; Gu, Y.; Zhao, Y.; Cui, Y.; Li, R.; et al. A nonmetallic plasmonic catalyst for photothermal CO₂ flow conversion with high activity, selectivity and durability. *Nat. Commun.* **2024**, *15*, 1273.
36. Ren, Y.; Fu, Y.; Li, N.; You, C.; Huang, J.; Huang, K.; Sun, Z.; Zhou, J.; Si, Y.; Zhu, Y.; et al. Concentrated solar CO₂ reduction in H₂O vapour with >1% energy conversion efficiency. *Nat. Commun.* **2024**, *15*, 4675.
37. Li, X.; Li, L.; Chu, X.; Liu, X.; Chen, G.; Guo, Q.; Zhang, Z.; Wang, M.; Wang, S.; Tahn, A.; et al. Photothermal CO₂ conversion to ethanol through photothermal heterojunction-nanosheet arrays. *Nat. Commun.* **2024**, *15*, 5639.
38. Liu, H.; Chen, B.; Chen, Y.; Zhou, M.; Tian, F.; Li, Y.; Jiang, J.; Zhai, W. Bioinspired self-standing, self-floating 3d solar evaporators breaking the trade-off between salt cycle and heat localization for continuous seawater desalination. *Adv. Mater.* **2023**, *35*, 2301596.
39. Yang, B.; Zhang, Z.; Liu, P.; Fu, X.; Wang, J.; Cao, Y.; Tang, R.; Du, X.; Chen, W.; Li, Z. Flatband λ -Ti₃O₅ towards extraordinary solar steam generation. *Nature* **2023**, *622*, 499–506.
40. Zou, H.; Meng, X.; Zhao, X.; Qiu, J. Hofmeister Effect-Enhanced Hydration Chemistry of Hydrogel for High-Efficiency Solar-Driven Interfacial Desalination. *Adv. Mater.* **2023**, *35*, 2207262.
41. Wang, J.; Sun, M.; Liu, C.; Ye, Y.; Chen, M.; Zhao, Z.; Zhang, Y.; Wu, X.; Wang, K.; Zhou, Y. Customized Microenvironments Spontaneously Facilitate Coupled Engineering of Real-Life Large-Scale Clean Water Capture and Pollution Remediation. *Adv. Mater.* **2023**, *35*, 2306103.
42. Xiang, B.; Gong, J.; Sun, Y.; Li, J. Robust PVA/GO@MOF membrane with fast photothermal self-cleaning property for oily wastewater purification. *J. Hazard. Mater.* **2024**, *462*, 132803.
43. Noureen, L.; Wang, Q.; Ismail, P.M.; Alomar, M.; Arshad, N.; Irshad, M.S.; Xu, Q.; Wang, X. Multifunctional aerogel with antibiofouling properties for efficient solar steam generation and seawater desalination. *Nano Today* **2024**, *54*, 102130.
44. Lv, C.; Bai, X.; Ning, S.; Song, C.; Guan, Q.; Liu, B.; Li, Y.; Ye, J. Nanostructured materials for photothermal carbon dioxide hydrogenation: Regulating solar utilization and catalytic performance. *ACS Nano* **2023**, *17*, 1725–1738.
45. Zhong, H.; Zhu, Z.; Lin, J.; Cheung, C.F.; Lu, V.L.; Yan, F.; Chan, C.-Y.; Li, G. Reusable and recyclable graphene masks with outstanding superhydrophobic and photothermal performances. *ACS Nano* **2020**, *14*, 6213–6221.
46. Tang, T.; Wang, Z.; Guan, J. Optimizing the Electrocatalytic Selectivity of Carbon Dioxide Reduction Reaction by Regulating the Electronic Structure of Single-Atom M-N-C Materials. *Adv. Funct. Mater.* **2022**, *32*, 2111504.
47. Ban, J.; Wen, X.; Xu, H.; Wang, Z.; Liu, X.; Cao, G.; Shao, G.; Hu, J. Dual Evolution in Defect and Morphology of Single-Atom Dispersed Carbon Based Oxygen Electrocatalyst. *Adv. Funct. Mater.* **2021**, *31*, 2010472.
48. Chen, M.; Zhang, H.; Li, H.; Zhao, Z.; Wang, K.; Zhou, Y.; Zhao, X.; Dubal, D.P. CxNy-based materials as gas sensors: Structure, performance, mechanism and perspective. *Coord. Chem. Rev.* **2024**, *503*, 215653.
49. Wang, T.; Chen, F.; Jiang, L.; Li, J.; Chen, K.; Gao, J. Metal-Organic-Framework-Derived Bromine and Nitrogen Dual-Doped Porous Carbon for CO₂ Photocycloaddition Reaction. *Inorg. Chem.* **2024**, *63*, 4224–4232.
50. Wang, T.; Chen, F.; An, H.; Chen, K.; Gao, J. Metal-organic-framework-derived boron and nitrogen dual-doped hollow mesoporous carbon for photo-thermal catalytic conversion of CO₂. *J. Solid. State Chem.* **2024**, *332*, 124570.
51. Liu, Y.; Chen, Y.; Liu, Y.; Chen, Z.; Yang, H.; Yue, Z.; Fang, Q.; Zhi, Y.; Shan, S. Zn and N co-doped porous carbon nanosheets for photothermally-driven CO₂ cycloaddition. *J. Catal.* **2022**, *407*, 65–76.
52. Yang, Z.; Xie, Y.; Feng, Y.; Yao, J. Tea saponin-derived porous carbon bearing rich oxygen-containing groups towards high efficient CO₂ fixation. *J. Environ. Chem. Eng.* **2024**, *12*, 112310.
53. Rong, W.; Ding, M.; Wang, Y.; Kong, S.; Yao, J. Porous biochar with a tubular structure for photothermal CO₂ cycloaddition: One-step doping versus two-step doping. *Sep. Purif. Technol.* **2025**, *353*, 128427.
54. Paliwal, K.S.; Sarkar, D.; Mitra, A.; Mahalingam, V. Chitosan-Derived N-Doped Carbon for Light-Mediated Carbon Dioxide Fixation into Epoxides. *ChemPlusChem.* **2023**, *88*, e202300448.
55. Qiao, B.; Wang, A.; Yang, X.; Allard, L.F.; Jiang, Z.; Cui, Y.; Liu, J.; Li, J.; Zhang, T. Single-atom catalysis of CO oxidation using Pt₁/FeO_x. *Nat. Chem.* **2011**, *3*, 634–641.
56. Yang, Q.; Yang, C.-C.; Lin, C.-H.; Jiang, H.-L. Metal-Organic-Framework-Derived Hollow N-Doped Porous Carbon with Ultrahigh Concentrations of Single Zn Atoms for Efficient Carbon Dioxide Conversion. *Angew. Chem. Int. Ed.* **2019**, *58*, 3511–3515.
57. Gong, L.; Sun, J.; Liu, Y.; Yang, G. Photoinduced synergistic catalysis on Zn single-atom-loaded hierarchical porous carbon for highly efficient CO₂ cycloaddition conversion. *J. Mater. Chem. A* **2021**, *9*, 21689–21694.
58. Yang, Q.; Peng, H.; Zhang, Q.; Qian, X.; Chen, X.; Tang, X.; Dai, S.; Zhao, J.; Jiang, K.; Yang, Q.; et al. Atomically Dispersed High-Density Al-N₄ Sites in Porous Carbon for Efficient Photodriven CO₂ Cycloaddition. *Adv. Mater.* **2021**, *33*, 2103186.
59. Dai, W.; Zou, M.; Long, J.; Li, B.; Zhang, S.; Yang, L.; Wang, D.; Mao, P.; Luo, S.; Luo, X. Nanoporous N-doped Carbon/ZnO hybrid derived from zinc aspartate: An acid-base bifunctional catalyst for efficient fixation of carbon dioxide

- into cyclic carbonates. *Appl. Surf. Sci.* **2021**, *540*, 148311.
60. Duan, C.; Ding, M.; Feng, Y.; Cao, M.; Yao, J. ZIF-L-derived ZnO/N-doped carbon with multiple active sites for efficient catalytic CO₂ cycloaddition. *Sep. Purif. Technol.* **2022**, *285*, 120359.
61. Tang, F.; Wang, L.; Ma, L.; Fang, Y.; Huang, J.; Liu, Y.-N. Protein-Zn(II) networks derived N-doped porous carbon-supported ZnS for photothermally catalytic CO₂ conversion. *J. CO₂ Util.* **2021**, *45*, 101431.
62. Xu, Y.; Wang, P.; Zhan, X.; Dai, W.; Li, Q.; Zou, J.; Luo, X. Enhancing the Lewis acidity of single atom Tb via introduction of boron to achieve efficient photothermal synergistic CO₂ cycloaddition. *J. Colloid. Interf. Sci.* **2024**, *673*, 134–142.
63. Wang, Q.; Ma, W.; Qian, J.; Li, N.; Zhang, C.; Deng, M.; Du, H. S-scheme towards interfacial charge transfer between POMs and MOFs for efficient visible-light photocatalytic Cr (VI) reduction. *Environ. Pollut.* **2024**, *347*, 123707.
64. Fang, Z.; Deng, Z.; Wan, X.; Li, Z.; Ma, X.; Hussain, S.; Ye, Z.; Peng, X. Keggin-type polyoxometalates molecularly loaded in Zr-ferrocene metal organic framework nanosheets for solar-driven CO₂ cycloaddition. *Appl. Catal. B-Environ.* **2021**, *296*, 120329.
65. He, J.; Li, J.; Han, Q.; Si, C.; Niu, G.; Li, M.; Wang, J.; Niu, J. Photoactive Metal-Organic Framework for the Reduction of Aryl Halides by the Synergistic Effect of Consecutive Photoinduced Electron-Transfer and Hydrogen-Atom-Transfer Processes. *ACS Appl. Mater. Inter.* **2019**, *12*, 2199–2206.
66. Chen, X.; Wei, M.; Yang, A.; Jiang, F.; Li, B.; Kholdeeva, O.A.; Wu, L. Near-Infrared Photothermal Catalysis for Enhanced Conversion of Carbon Dioxide under Mild Conditions. *ACS Appl. Mater. Inter.* **2022**, *14*, 5194–5202.
67. Wang, T.; Zhu, Y.; Wang, W.; Niu, J.; Lu, Z.; He, P. Polyoxometalates coupled covalent organic frameworks as highly active photothermal nanoreactor for CO₂ cycloaddition. *Nano Res.* **2024**, *17*, 5975–5984.
68. Dutta, S.; Mukherjee, S.; Qazvini, O.T.; Gupta, A.K.; Sharma, S.; Mahato, D.; Babarao, R.; Ghosh, S.K. Three-in-One C₂H₂-Selectivity-Guided Adsorptive Separation across an Isoreticular Family of Cationic Square-Lattice MOFs. *Angew. Chem. Int. Ed.* **2022**, *61*, e202114132.
69. Belmabkhout, Y.; Guillemin, V.; Eddaoudi, M. Low concentration CO₂ capture using physical adsorbents: Are metal-organic frameworks becoming the new benchmark materials? *Chem. Eng. J.* **2016**, *296*, 386–397.
70. Dong, A.; Chen, D.; Li, Q.; Qian, J. Metal-organic frameworks for greenhouse gas applications. *Small* **2023**, *19*, 2201550.
71. Ma, C.; Urban, J.J. Hydrogen-bonded polyimide/metal-organic framework hybrid membranes for ultrafast separations of multiple gas pairs. *Adv. Funct. Mater.* **2019**, *29*, 1903243.
72. Gao, W.-Y.; Chen, Y.; Niu, Y.; Williams, K.; Cash, L.; Perez, P.J.; Wojtas, L.; Cai, J.; Chen, Y.S.; Ma, S. Crystal engineering of an nbo topology metal-organic framework for chemical fixation of CO₂ under ambient conditions. *Angew. Chem. Int. Ed.* **2014**, *53*, 2615–2619.
73. Li, P.-Z.; Wang, X.-J.; Liu, J.; Lim, J.S.; Zou, R.; Zhao, Y. A triazole-containing metal-organic framework as a highly effective and substrate size-dependent catalyst for CO₂ conversion. *J. Am. Chem. Soc.* **2016**, *138*, 2142–2145.
74. Yang, D.-A.; Cho, H.-Y.; Kim, J.; Yang, S.-T.; Ahn, W.-S. CO₂ capture and conversion using Mg-MOF-74 prepared by a sonochemical method. *Energ. Environ. Sci.* **2012**, *5*, 6465–6473.
75. Shi, Y.; Zhao, J.; Xu, H.; Hou, S.-L.; Zhao, B. Eco-friendly co-catalyst-free cycloaddition of CO₂ and aziridines activated by a porous MOF catalyst. *Sci. China Chem.* **2021**, *64*, 1316–1322.
76. Zou, R.; Li, P.-Z.; Zeng, Y.-F.; Liu, J.; Zhao, R.; Duan, H.; Luo, Z.; Wang, J.-G.; Zou, R.; Zhao, Y. Bimetallic Metal-Organic Frameworks: Probing the Lewis Acid Site for CO₂ Conversion. *Small* **2016**, *12*, 2334–2343.
77. Chen, Y.; Li, F.; Liu, L.; Zhou, Y.-H. Implanting multi-functional ionic liquids into MOF nodes for boosting CO₂ cycloaddition under solventless and cocatalyst-free conditions. *Chem. Eng. J.* **2024**, *490*, 151657.
78. Sharma, N.; Dhankhar, S.S.; Nagaraja, C.M. A Mn(II)-porphyrin based metal-organic framework (MOF) for visible-light-assisted cycloaddition of carbon dioxide with epoxides. *Microporous Mesoporous Mater.* **2019**, *280*, 372–378.
79. Jiang, L.; Wu, D.; Huang, Z.; Chen, F.; Chen, K.; Ibragimov, A.B.; Gao, J. In Situ Pyrolysis of ZIF-67 to Construct Co₂N_{0.67}@ZIF-67 for Photocatalytic CO₂ Cycloaddition Reaction. *Inorg. Chem.* **2024**, *63*, 14761–14769.
80. Wang, Y.; Ding, M.; Rong, W.; Kong, S.; Yao, J. In situ growth of Fe-doped zeolitic imidazolate framework on MXene for boosting photodriven CO₂ cycloaddition. *Sep. Purif. Technol.* **2024**, *345*, 127399.
81. Wu, Y.; Gao, L.; Zhou, X.-C.; Yu, X.; Meng, Y.-R.; Zuo, J.-L.; Su, J.; Yuan, S. Designing photothermal catalytic systems in multi-component MOFs for enhanced conversion of carbon dioxide. *Chem. Commun.* **2024**, *60*, 9825–9828.
82. Tu, X.; Sun, C.; Hu, Y.; Chen, Y.; Zhu, S.; Qu, J.; Zhu, Z.; Zhang, X.; Zheng, H. Bimetallic Fe/Co photothermal catalyst for fixing CO₂ to cyclic carbonates under atmospheric pressure. *Catal. Sci. Technol.* **2024**, *14*, 3201–3210.
83. Duan, C.; Xie, Y.; Ding, M.; Feng, Y.; Yao, J. Design of carbonized melamine sponge@MOFs composites bearing diverse acid-base properties for boosting thermal and solar-driven CO₂ cycloaddition. *J. CO₂ Util.* **2022**, *64*, 102158.
84. Lyu, H.; Li, H.; Hanikel, N.; Wang, K.; Yaghi, O.M. Covalent organic frameworks for carbon dioxide capture from air. *J. Am. Chem. Soc.* **2022**, *144*, 12989–12995.
85. Kurisingal, J.F.; Kim, H.; Choe, J.H.; Hong, C.S. Covalent organic framework-based catalysts for efficient CO₂ utilization

- reactions. *Coord. Chem. Rev.* **2022**, *473*, 214835.
86. Wu, Q.-J.; Liang, J.; Huang, Y.-B.; Cao, R. Thermo-, Electro-, and Photocatalytic CO₂ Conversion to Value-Added Products over Porous Metal/Covalent Organic Frameworks. *Acc. Chem. Res.* **2022**, *55*, 2978–2997.
87. Ding, L.-G.; Yao, B.-J.; Wu, W.-X.; Yu, Z.-G.; Wang, X.-Y.; Kan, J.-L.; Dong, Y.-B. Metalloporphyrin and Ionic Liquid-Functionalized Covalent Organic Frameworks for Catalytic CO₂ Cycloaddition via Visible-Light-Induced Photothermal Conversion. *Inorg. Chem.* **2021**, *60*, 12591–12601.
88. Kondrat, S.; Feng, G.; Bresme, F.; Urbakh, M.; Kornyshev, A.A. Theory and simulations of ionic liquids in nanoconfinement. *Chem. Rev.* **2023**, *123*, 6668–6715.
89. Li, X.; Chen, K.; Guo, R.; Wei, Z. Ionic liquids functionalized MOFs for adsorption. *Chem. Rev.* **2023**, *123*, 10432–10467.
90. Fang, X.; Yang, L.; Dai, Z.; Cong, D.; Zheng, D.; Yu, T.; Tu, R.; Zhai, S.; Yang, J.; Song, F.; Wu, H.; Deng, W.-Q.; Liu, C. Poly (ionic liquid) s for Photo-Driven CO₂ Cycloaddition: Electron Donor–Acceptor Segments Matter. *Adv. Sci.* **2023**, *2206687*.
91. Liu, Y.; Sun, J.; Huang, H.; Bai, L.; Zhao, X.; Qu, B.; Xiong, L.; Bai, F.; Tang, J.; Jing, L. Improving CO₂ photoconversion with ionic liquid and Co single atoms. *Nat. Commun.* **2023**, *14*, 1457.
92. Guo, Y.; Chen, W.; Feng, L.; Fan, Y.; Liang, J.; Wang, X.; Zhang, X. Greenery-inspired nanoengineering of bamboo-like hierarchical porous nanotubes with spatially organized bifunctionalities for synergistic photothermal catalytic CO₂ fixation. *J. Mater. Chem. A.* **2022**, *10*, 12418–12428.
93. Guo, Q.; Xia, S.-G.; Li, X.-B.; Wang, Y.; Liang, F.; Lin, Z.-S.; Tung, C.-H.; Wu, L.-Z. Flower-like cobalt carbide for efficient carbon dioxide conversion. *Chem. Commun.* **2020**, *56*, 7849–7852.
94. Fang, Z.; Wang, Y.; Hu, Y.; Yao, B.; Ye, Z.; Peng, X. A CO₂-philic ferrocene-based porous organic polymer for solar-driven CO₂ conversion from flue gas. *J. Mater. Chem. A* **2023**, *11*, 18272–18279.
95. Tailor, N.K.; Singh, S.; Saini, S.K.; Kaivalya; Afroz, M.A.; Kumar, M.; Peter, S.C.; Pant, K.K.; Satapathi, S. Unveiling the Potential of Halide Perovskites for Seasonally Adaptive CO₂ Photoreduction under Low Light Conditions. *Adv. Funct. Mater.* **2024**, *34*, 2402894.
96. Bi, W.; Hu, Y.; Jiang, H.; Zhang, L.; Li, C. Revealing the sudden alternation in Pt@ h-BN nanoreactors for nearly 100 % CO₂-to-CH₄ photoreduction. *Adv. Funct. Mater.* **2021**, *31*, 2010780.
97. Xu, Y.; Ren, Y.; Zhou, G.; Feng, S.; Yang, Z.; Dai, S.; Lu, Z.; Zhou, T. Amide-Engineered Metal-Organic Porous Liquids Toward Enhanced CO₂ Photoreduction Performance. *Adv. Funct. Mater.* **2024**, *34*, 2313695.
98. Dong, M.; Zhou, J.; Zhong, J.; Li, H.T.; Sun, C.-Y.; Han, Y.-D.; Kou, J.-N.; Kang, Z.-H.; Wang, X.-L.; Su, Z.-M. CO₂ dominated bifunctional catalytic sites for efficient industrial exhaust conversion. *Adv. Funct. Mater.* **2022**, *32*, 2110136.
99. Saini, N.; Malik, A.; Jain, S.L. Light driven chemical fixation and conversion of CO₂ into cyclic carbonates using transition metals: A review on recent advancements. *Coord. Chem. Rev.* **2024**, *502*, 215636.
100. Tan, C.-L.; Qi, M.-Y.; Tang, Z.-R.; Xu, Y.-J. Isolated Single-Atom Cobalt in the ZnIn₂S₄ Monolayer with Exposed Zn Sites for CO₂ Photofixation. *ACS Catal.* **2023**, *13*, 8317–8329.
101. Prajapati, P.K.; Kumar, A.; Jain, S.L. First Photocatalytic Synthesis of Cyclic Carbonates from CO₂ and Epoxides Using CoPc/TiO₂ Hybrid under Mild Conditions. *ACS Sustain. Chem. Eng.* **2018**, *6*, 7799–7809.
102. Bakiro, M.; Hussein Ahmed, S.; Alzamy, A. Efficient Visible-Light Photocatalytic Cycloaddition of CO₂ and Propylene Oxide Using Reduced Graphene Oxide Supported BiNbO₄. *ACS Sustain. Chem. Eng.* **2020**, *8*, 12072–12079.
103. Gong, X.; Zhang, Y.; Xu, Y.; Zhai, G.; Liu, X.; Bao, X.; Wang, Z.; Liu, Y.; Wang, P.; Cheng, H.; et al. Synergistic Effect between CO₂ Chemisorption Using Amino-Modified Carbon Nitride and Epoxide Activation by High-Energy Electrons for Plasmon-Assisted Synthesis of Cyclic Carbonates. *ACS Appl. Mater. Interfaces* **2022**, *14*, 51029–51040.
104. Kumar, A.; Samanta, S.; Srivastava, R. Graphitic Carbon Nitride Modified with Zr-Thiamine Complex for Efficient Photocatalytic CO₂ Insertion to Epoxide: Comparison with Traditional Thermal Catalysis. *ACS Appl. Nano Mater.* **2021**, *4*, 6805–6820.
105. Cheng, R.; Wang, A.; Sang, S.; Liang, H.; Liu, S.; Tsiakaras, P. Photocatalytic CO₂ cycloaddition over highly efficient W₁₈O₄₉-based composites: An economic and ecofriendly choice. *Chem. Eng. J.* **2023**, *466*, 142982.
106. Jiang, H.; Zang, C.; Guo, L.; Gao, X. Carbon vacancies enriched carbon nitride nanotubes for Pd coordination environment optimization: Highly efficient photocatalytic hydrodechlorination and CO₂ cycloaddition. *Sci. Total Environ.* **2022**, *838*, 155920.
107. Elgohary, E.A.; Mohamed, Y.M.A.; Rabie, S.T.; Salih, S.A.; Fekry, A.M.; El Nazer, H.A. Highly selective visible-light-triggered CO₂ fixation to cyclic carbonates under mild conditions using TiO₂/multiwall carbon nanotubes (MWCNT) grafted with Pt or Pd nanoparticles. *New J. Chem.* **2021**, *45*, 17301–17312.
108. Alzard, R.H.; Siddig, L.A.; Abdelhamid, A.S.; Ramachandran, T.; Alzamy, A. Structural analysis and photocatalytic activities of bismuth-lanthanide oxide perovskites. *J. Solid. State Chem.* **2024**, *329*, 124359.
109. Khalid, A.; Razzaq, Z.; Ahmad, P.; Al-Anzi, B.S.; Rehman, F.; Muhammad, S.; Khandaker, M.U.; Albasher, G.; Alsultan, N.; Liaqat, I.; et al. Visible-light promoted chemical fixation of carbon dioxide with epoxide into cyclic carbonates over

- S-scheme CdS-CeO₂ photocatalyst. *Mater. Sci. Semicond. Process.* **2023**, *165*, 107649.
110. Li, G.; Sui, X.; Cai, X.; Hu, W.; Liu, X.; Chen, M.; Zhu, Y. Precisely constructed silver active sites in gold nanoclusters for chemical fixation of CO₂. *Angew. Chem. Int. Ed.* **2021**, *133*, 10667–10670.
 111. Wong, K.T.; Brigljević, B.; Lee, J.H.; Yoon, S.Y.; Jang, S.B.; Choong, C.E.; Nah, I.; Kim, H.; Roh, H.-S.; Kwak, S.K. Highly Exposed NH₂ Edge on Fragmented g-C₃N₄ Framework with Integrated Molybdenum Atoms for Catalytic CO₂ Cycloaddition: DFT and Techno-Economic Assessment. *Small* **2023**, *19*, 2204336.
 112. Liu, C.; Niu, H.; Wang, D.; Gao, C.; Said, A.; Liu, Y.; Wang, G.; Tung, C.-H.; Wang, Y. S-Scheme Bi-oxide/Ti-oxide Molecular Hybrid for Photocatalytic Cycloaddition of Carbon Dioxide to Epoxides. *ACS Catal.* **2022**, *12*, 8202–8213.
 113. Wang, D.; Said, A.; Liu, Y.; Niu, H.; Liu, C.; Wang, G.; Li, Z.; Tung, C.-H.; Wang, Y. Cr-Ti Mixed Oxide Molecular Cages: Synthesis, Structure, Photoresponse, and Photocatalytic Properties. *Inorg. Chem.* **2022**, *61*, 14887–14898.
 114. Said, A.; Zhang, G.; Wang, D.; Chen, G.; Liu, Y.; Gao, F.; Tung, C.-H.; Wang, Y. Divalent Heterometal Doped Titanium-Oxide Cluster Polymers: Structures, Photoresponse, and Photocatalysis. *Inorg. Chem.* **2023**, *62*, 13476–13484.
 115. Bakiro, M.; Ahmed, S.H.; Alzamy, A. Cycloaddition of CO₂ to propylene oxide using BiNbO₄/NH₂-MIL-125(Ti) composites as visible-light photocatalysts. *J. Environ. Chem. Eng.* **2020**, *8*, 104461.
 116. Hussein Ahmed, S.; Bakiro, M.; Alzamy, A. Photocatalytic Activities of FeNbO₄/NH₂-MIL-125(Ti) Composites toward the Cycloaddition of CO₂ to Propylene Oxide. *Molecules* **2021**, *26*, 1693.
 117. Erzina, M.; Guselnikova, O.; Elashnikov, R.; Trelin, A.; Zabelin, D.; Postnikov, P.; Siegel, J.; Zabelina, A.; Ulbrich, P.; Kolska, Z.; et al. BioMOF coupled with plasmonic CuNPs for sustainable CO₂ fixation in cyclic carbonates at ambient conditions. *J. CO₂ Util.* **2023**, *69*, 102416.
 118. Hu, Y.; Abazari, R.; Sanati, S.; Nadafan, M.; Carpenter-Warren, C.L.; Slawin, A.M.Z.; Zhou, Y.; Kirillov, A.M. A Dual-Purpose Ce(III)-Organic Framework with Amine Groups and Open Metal Sites: Third-Order Nonlinear Optical Activity and Catalytic CO₂ Fixation. *ACS Appl. Mater. Interfaces* **2023**, *15*, 37300–37311.
 119. Payra, S.; Roy, S. From Trash to Treasure: Probing Cycloaddition and Photocatalytic Reduction of CO₂ over Cerium-Based Metal-Organic Frameworks. *J. Phys. Chem. C* **2021**, *125*, 8497–8507.
 120. He, Y.; Xu, M.; Xia, J.; Zhang, C.; Song, X.; Zhao, X.; Fu, M.; Li, S.; Liu, X. Effect of exposed active sites of semi-amorphous Fe-BTC on photocatalytic CO₂ cycloaddition reaction under ambient conditions. *Mol. Catal.* **2023**, *542*, 113134.
 121. Zhang, H.; Si, S.; Zhai, G.; Li, Y.; Liu, Y.; Cheng, H.; Wang, Z.; Wang, P.; Zheng, Z.; Dai, Y.; et al. The long-distance charge transfer process in ferrocene-based MOFs with FeO₆ clusters boosts photocatalytic CO₂ chemical fixation. *Appl. Catal. B-Environ.* **2023**, *337*, 122909.
 122. Shi, Q.; Chen, M.-H.; Xiong, J.; Li, T.; Feng, Y.-Q.; Zhang, B. Porphyrin-Based Two-Dimensional Metal-Organic framework nanosheets for efficient photocatalytic CO₂ transformation. *Chem. Eng. J.* **2024**, *481*, 148301.
 123. Siddig, L.A.; Alzard, R.H.; Nguyen, H.L.; Göb, C.R.; Alnaqbi, M.A.; Alzamy, A. Hexagonal Layer Manganese Metal-Organic Framework for Photocatalytic CO₂ Cycloaddition Reaction. *ACS Omega* **2022**, *7*, 9958–9963.
 124. Carrasco, S.; Orcajo, G.; Martínez, F.; Imaz, I.; Kavak, S.; Arenas-Esteban, D.; MasPOCH, D.; Bals, S.; Calleja, G.; Horcajada, P. Hf/porphyrin-based metal-organic framework PCN-224 for CO₂ cycloaddition with epoxides. *Mater. Today Adv.* **2023**, *19*, 100390.
 125. Liang, J.; Jiang, X.; Zhang, X.; Yu, H.; Shi, J.; Wang, M. Co-porphyrin-based metal-organic framework for light-driven efficient green conversion of CO₂ and epoxides. *Chem. Eng. J.* **2024**, *499*, 156428.
 126. Zhai, G.; Liu, Y.; Mao, Y.; Zhang, H.; Lin, L.; Li, Y.; Wang, Z.; Cheng, H.; Wang, P.; Zheng, Z.; et al. Improved photocatalytic CO₂ and epoxides cycloaddition via the synergistic effect of Lewis acidity and charge separation over Zn modified UiO-bpydc. *Appl. Catal. B-Environ.* **2022**, *301*, 120793.
 127. Zhai, G.; Liu, Y.; Lei, L.; Wang, J.; Wang, Z.; Zheng, Z.; Wang, P.; Cheng, H.; Dai, Y.; Huang, B. Light-Promoted CO₂ Conversion from Epoxides to Cyclic Carbonates at Ambient Conditions over a Bi-Based Metal-Organic Framework. *ACS Catal.* **2021**, *11*, 1988–1994.
 128. Li, Y.; Zhai, G.; Liu, Y.; Wang, Z.; Wang, P.; Zheng, Z.; Cheng, H.; Dai, Y.; Huang, B. Synergistic effect between boron containing metal-organic frameworks and light leading to enhanced CO₂ cycloaddition with epoxides. *Chem. Eng. J.* **2022**, *437*, 135363.
 129. Li, L.; Liu, W.; Shi, T.; Shang, S.; Zhang, X.; Wang, H.; Tian, Z.; Chen, L.; Xie, Y. Photoexcited Single-Electron Transfer for Efficient Green Synthesis of Cyclic Carbonate from CO₂. *ACS Mater. Lett.* **2023**, *5*, 1219–1226.
 130. Huang, Z.-W.; Hu, K.-Q.; Mei, L.; Wang, C.-Z.; Chen, Y.-M.; Wu, W.-S.; Chai, Z.-F.; Shi, W.-Q. Potassium Ions Induced Framework Interpenetration for Enhancing the Stability of Uranium-Based Porphyrin MOF with Visible-Light-Driven Photocatalytic Activity. *Inorg. Chem.* **2020**, *60*, 651–659.
 131. Fan, S.-C.; Chen, S.-Q.; Wang, J.-W.; Li, Y.-P.; Zhang, P.; Wang, Y.; Yuan, W.; Zhai, Q.-G. Precise Introduction of Single Vanadium Site into Indium-Organic Framework for CO₂ Capture and Photocatalytic Fixation. *Inorg. Chem.* **2022**, *61*, 14131–14139.
 132. Liu, L.; Zhang, J.; Cheng, X.; Xu, M.; Kang, X.; Wan, Q.; Han, B.; Wu, N.; Zheng, L.; Ma, C. Amorphous NH₂-MIL-68

- as an efficient electro- and photo-catalyst for CO₂ conversion reactions. *Nano Res.* **2022**, *16*, 181–188.
133. Xie, X.; Li, H.; Cao, W.; Ke, D.; Dong, Z.; Tian, L.; Xiong, X.; Zhang, J. A bifunctional catalyst derived from copper metal-organic framework for highly selective photocatalytic CO₂ reduction and CO₂ cycloaddition reaction. *J. Mol. Struct.* **2024**, *1312*, 138556.
 134. Sun, W.; Zhu, J.; Zhang, M.; Meng, X.; Chen, M.; Feng, Y.; Chen, X.; Ding, Y. Recent advances and perspectives in cobalt-based heterogeneous catalysts for photocatalytic water splitting, CO₂ reduction, and N₂ fixation. *Chin. J. Catal.* **2022**, *43*, 2273–2300.
 135. Xu, M.L.; Lu, M.; Qin, G.-Y.; Wu, X.-M.; Yu, T.; Zhang, L.-N.; Li, K.; Cheng, X.; Lan, Y.-Q. Piezo-photocatalytic synergy in BiFeO₃@ COF Z-scheme heterostructures for high-efficiency overall water splitting. *Angew. Chem. Int. Ed.* **2022**, *134*, e202210700.
 136. Li, X.; Niu, X.; Fu, P.; Song, Y.; Zhang, E.; Dang, Y.; Yan, J.; Feng, G.; Lei, S.; Hu, W. Macrocyclic-on-COF photocatalyst constructed by in-situ linker exchange for efficient photocatalytic CO₂ cycloaddition. *Appl. Catal. B-Environ.* **2024**, *350*, 123943.
 137. Xiong, J.; Chen, M.-H.; Li, X.-Y.; Shi, Q.; Xu, Y.-H.; Feng, Y.-Q.; Zhang, B. Metalloporphyrin-based covalent triazine frameworks for efficient photocatalytic CO₂ cycloaddition at ambient conditions. *Dyes Pigm.* **2025**, *233*, 112531.
 138. Qiu, L.-Q.; Li, H.-R.; He, L.-N. Incorporating catalytic units into nanomaterials: Rational design of multipurpose catalysts for CO₂ valorization. *Acc. Chem. Res.* **2023**, *56*, 2225–2240.
 139. Giri, A.; Patra, A. Porous organic polymers: Promising testbed for heterogeneous reactive oxygen species mediated photocatalysis and nonredox CO₂ fixation. *Chem. Rec.* **2022**, *22*, e202200071.
 140. Bao, Y.; Liu, J.; Zhang, Y.; Zheng, L.; Ma, J.; Zhang, F.; Xiong, Y.; Meng, X.; Dai, Z.; Xiao, F.-S. Porous organic polymers with diverse quaternary phosphonium units for chemical fixation of CO₂ with low concentration. *Fuel* **2023**, *331*, 125909.
 141. Sarkar, C.; Paul, R.; Dao, D.Q.; Xu, S.; Chatterjee, R.; Shit, S.C.; Bhaumik, A.; Mondal, J. Unlocking Molecular Secrets in a Monomer-Assembly-Promoted Zn-Metalated Catalytic Porous Organic Polymer for Light-Responsive CO₂ Insertion. *ACS Appl. Mater. Interfaces* **2022**, *14*, 37620–37636.
 142. Cui, C.; Sa, R.; Hong, Z.; Zhong, H.; Wang, R. Ionic-liquid-modified click-based porous organic polymers for controlling capture and catalytic conversion of CO₂. *ChemSusChem* **2020**, *13*, 180–187.
 143. Jingyi, Y.; Siqi, S.; Huaitao, P.; Qihao, Y.; Liang, C. Integration of Atomically Dispersed Ga Sites with C₃N₄ Nanosheets for Efficient Photo-driven CO₂ Cycloaddition. *Chem. J. Chin. U* **2022**, *43*.
 144. Wang, Y.; Liu, H.; Shi, Q.; Miao, Z.; Duan, H.; Wang, Y.; Rong, H.; Zhang, J. Single-Atom Titanium on Mesoporous Nitrogen, Oxygen-Doped Carbon for Efficient Photo-thermal Catalytic CO₂ Cycloaddition by a Radical Mechanism. *Angew. Chem. Int. Ed.* **2024**, *63*, e202404911.
 145. Zhang, H.; Zhai, G.; Lei, L.; Zhang, C.; Liu, Y.; Wang, Z.; Cheng, H.; Zheng, Z.; Wang, P.; Dai, Y.; et al. Photo-induced photo-thermal synergy effect leading to efficient CO₂ cycloaddition with epoxide over a Fe-based metal organic framework. *J. Colloid. Interf. Sci.* **2022**, *625*, 33–40.
 146. Zhou, X.; Zhang, H.; Cheng, H.; Wang, Z.; Wang, P.; Zheng, Z.; Dai, Y.; Xing, D.; Liu, Y.; Huang, B. Enhanced cycloaddition between CO₂ and epoxide over a bismuth-based metal organic framework due to a synergistic photocatalytic and photothermal effect. *J. Colloid. Interf. Sci.* **2024**, *658*, 805–814.
 147. Jiang, B.; Zhang, C.; Yang, N.; Zhou, Q.; Zhang, L.; Li, J.; Yang, W.; Yang, X.; Zhang, L. 2D/2D ZIF-L-Derived Zn^{δ+} (0 ≤ δ ≤ 2) and N Codoped Carbon Skeleton@ZnIn₂S₄ S-Scheme Heterojunction for Solar-Driven CO₂ Cycloaddition. *ACS Sustain. Chem. Eng.* **2024**, *12*, 6584–6595.
 148. Lu, W.; Shi, X.; Zhou, H.; Luo, W.; Wang, L.; He, H. Tailoring and properties of a novel solar energy-triggered regenerative bionic fiber adsorbent for CO₂ capture. *Chem. Eng. J.* **2022**, *449*, 137885.
 149. Tang, Z.; Zhu, F.; Zhou, J.; Chen, W.; Wang, K.; Liu, M.; Wang, N.; Li, N. Monolithic NF@ ZnO/Au@ ZIF-8 photocatalyst with strong photo-thermal-magnetic coupling and selective-breathing effects for boosted conversion of CO₂ to CH₄. *Appl. Catal. B-Environ.* **2022**, *309*, 121267.
 150. Li, D.; Sun, J.; Ma, R.; Wei, J. High-efficient solar-driven hydrogen production by full-spectrum synergistic photo-thermo-catalytic methanol steam reforming with in-situ photoreduced Pt-CuO_x catalyst. *J. Energy Chem.* **2022**, *71*, 460–469.
 151. Xu, Y.; Liu, M.; Tong, F.; Ma, F.; He, X.; Wang, Z.; Wang, P.; Liu, Y.; Cheng, H.; Dai, Y. Strain-assisted in-situ formed oxygen defective WO₃ film for photothermal-synergistic reverse water gas shift reaction and single-particle study. *Chem. Eng. J.* **2022**, *433*, 134199.
 152. Wu, Y.; Yu, X.-F.; Du, Y.; Xia, L.; Guo, Q.; Zhang, K.; Zhang, W.; Liu, S.; Peng, Y.; Li, Z.; et al. A combination of two swords thermo-blue-light-synergistic-catalytic CO₂ cycloaddition on ZnIn₂S₄ exposed abundant of Zinc cation sites. *Appl. Catal. B-Environ.* **2023**, *331*, 122732.
 153. Zhang, W.; Li, Z.; Yu, X.-F.; Zhang, K.; Liu, S.; Du, Y.; Guo, Q.; Zhang, L.; Ding, X.; Tang, H.; et al. Photothermal Synergistic Catalysis over Defective Zn₃In₂S₆ for CO₂ Fixation. *Inorg. Chem.* **2024**, *63*, 2954–2966.
 154. Tu, X.; Sun, Q.; Zhu, S.; Sun, C.; Hu, Y.; Qu, J.; Zhu, Z.; Duan, X.; Zhang, X.; Zheng, H. Nanoflower Fe-base complex

- for efficient CO₂ fixation under atmospheric pressure. *J. Environ. Chem. Eng.* **2024**, *12*, 112544.
155. Zhang, L.; Tu, X.; Chen, Y.; Zhu, S.; Sun, C.; Song, Y.; Zheng, H. Synthesis of cyclic carbonates by photothermal catalytic coupling of CO₂ and epoxides under solvent-free conditions. *Appl. Catal. A-Gen.* **2023**, *666*, 119435.
156. Zhang, L.; Tu, X.; Chen, Y.; Han, W.; Chen, L.; Sun, C.; Zhu, S.; Song, Y.; Zheng, H. Photothermal catalysis without solvent for fixing CO₂ to cyclic carbonate. *Mol. Catal.* **2023**, *538*, 112971.